*Progress In Electromagnetics Research, PIER 11, 51–102, 1995*

# MOL-BPM METHOD OF LINES BASED BEAM PROPGAGATION METHOD

*R. Pregla*



## 1. Introduction

The method of lines (MoL) which is a special finite difference method has been proved to be especially suited for the analysis of wave propagation in multilayered waveguide structures. In general the MoL was introduced to solve partial differential equations in different fields of science [1]. In the author's group the MoL was used for

the analysis of the wave propagation in waveguides for microwave integrated circuits [2]. Then the MoL was systematically developed for multilayered microwave and millimeter wave structures [3–5]. With the paper [6] the background was given for the analysis of waveguides for integrated optics [7,8].

To analyze longitudinal inhomogeneous optical waveguides the most efficient method is the beam propagation method (BPM) introduced by Feit and Fleck [9].

An important condition for the development of a propagation algorithm based on the MoL was the introduction of absorbing boundary condition [10] into the MoL by the author [11]. Examples of application are demonstrated in [11–14]. Further details of ABCs for the MoL are given in [15]. An improved approach is described in this article. An alternative possibility to handle the radiated field was introduced by G. R. Hadley. He has developed the so called transparent boundary conditions [16,17] which are very important especially for FD-BPM algorithms.

The first 2D-MoL-BPM solution that means for slab guides as an exact eigenmode solution was used by Gerdes [11]. This is a specialized formulation of the general solution given for inhomogeneous dielectric layers in [3,6]. The 3D algorithm introduced by the author was first demonstrated at the IPR in 1990. Both algorithms are published in [18]. The MoL-BPM is an inherent algorithm based on eigenmode expansion not only of guided modes but also of radiation modes. Also in the case of the split step algorithm eigenmodes are used for the propagation in the reference medium [19]. The MoL-BPM has also been extended to reflected waves [20]. Special algorithms are developed e.g. for curved waveguides [21]. This paper also gives the principle of the algorithm for the vectorial MoL-BPM.

In this contribution the MoL-BPM algorithms are described in a unified form. Only some typical numerical results will be presented. For the other results the reader may be referred to the literature.

## 2. Analysis

### *2.1 Basic Equations*

The cross sections of optical waveguides are inhomogeneous according to the material. Figure 2.1 shows a strip loaded slab guide as

example. The refractive index $n$ or the permittivity $\epsilon_r$ is a function of both coordinate directions $x$ and $y$ of the cross section

$$\epsilon_r = \epsilon_r(x, y) \tag{2.1}$$

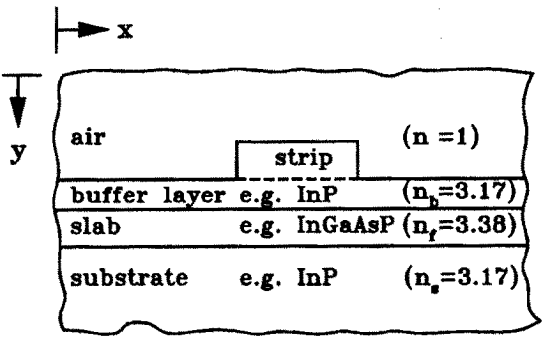


**Figure 2.1 Strip loaded slab guide.**

To calculate the electromagnetic field we therefore follow the way described by Collin [20]. The magnetic field will be determined by the curl of the magnetic potential $\mathbf{\Pi}$

$$\eta_0 \boldsymbol{H} = jk_0^{-1} \nabla \times \mathbf{\Pi} \tag{2.2}$$

where $k_0$ and $\eta_0$ are the wave number and the wave impedance of free space. Different from [20] we assume, that the vector $\mathbf{\Pi}$ has two components, one in $x$ and the other in $y$ direction

$$\mathbf{\Pi} = \phi_e \boldsymbol{a}_x + \phi_h \boldsymbol{a}_y \tag{2.3}$$

according to the $x$ and $y$ dependence of the permittivity. $\boldsymbol{a}_x$ and $\boldsymbol{a}_y$ are unit vectors in $x$ and $y$ directions respectively. The magnetic potential has to fulfill the wave equation

$$\nabla^2 \mathbf{\Pi} - \epsilon_r^{-1} (\nabla \epsilon_r) \nabla \cdot \mathbf{\Pi} + \epsilon_r k_0^2 \mathbf{\Pi} = 0 \tag{2.4}$$

With the scalar potentials $\phi_e$ and $\phi_h$ from Eq. (2.3) we obtain two coupled scalar wave equations

$$\Delta\phi_e - \epsilon_r^{-1} \frac{\partial \epsilon_r}{\partial x} \frac{\partial \phi_e}{\partial x} + \epsilon_r k_0^2 \phi_e = \epsilon_r^{-1} \frac{\partial \epsilon_r}{\partial x} \frac{\partial \phi_h}{\partial y} \tag{2.5}$$

$$\Delta\phi_h - \epsilon_r^{-1} \frac{\partial \epsilon_r}{\partial y} \frac{\partial \phi_h}{\partial y} + \epsilon_r k_0^2 \phi_h = \epsilon_r^{-1} \frac{\partial \epsilon_r}{\partial y} \frac{\partial \phi_e}{\partial x} \tag{2.6}$$

The electric field may be derived from $\mathbf{\Pi}$ by

$$\boldsymbol{E} = \epsilon_r^{-1} k_0^{-2} \nabla \times \nabla \times \mathbf{\Pi} \tag{2.7}$$

Because $\epsilon_r \boldsymbol{E}$ is obtained with the curl operator from a vector field the Maxwell's equation $\operatorname{div} \boldsymbol{D} = 0$ is automatically fulfilled. This is an important advantage of the used formulation. The components of the field are given by

$$\begin{aligned}
\eta_0 H_x &= -j \frac{\partial \phi_h}{\partial \overline{z}} \\
\eta_0 H_y &= j \frac{\partial \phi_e}{\partial \overline{z}} \\
\eta_0 H_z &= j \frac{\partial \phi_h}{\partial \overline{x}} - j \frac{\partial \phi_e}{\partial \overline{y}} \\
\epsilon_r E_x &= \frac{\partial^2 \phi_h}{\partial \overline{x} \partial \overline{y}} - \frac{\partial^2 \phi_e}{\partial \overline{y}^2} - \frac{\partial^2 \phi_e}{\partial \overline{z}^2} \\
\epsilon_r E_y &= \frac{\partial^2 \phi_e}{\partial \overline{x} \partial \overline{y}} - \frac{\partial^2 \phi_h}{\partial \overline{x}^2} - \frac{\partial^2 \phi_h}{\partial \overline{z}^2} \\
\epsilon_r E_z &= \frac{\partial^2 \phi_e}{\partial \overline{x} \partial \overline{z}} + \frac{\partial^2 \phi_h}{\partial \overline{y} \partial \overline{z}}
\end{aligned} \tag{2.8}$$

In these equations we have used normalized coordinates: $\overline{x} = k_0 x$, $\overline{y} = k_0 y$, $\overline{z} = k_0 z$. Scalar equations are obtained by $\phi_e = 0$ or $\phi_h = 0$. According to the $x$ direction we obtain quasi TE modes with $\phi_e \neq 0$, $\phi_h = 0$ and quasi TM modes with $\phi_e = 0$, $\phi_h \neq 0$. The scalar wave equations for these modes are

$$\frac{\partial^2}{\partial \overline{z}^2} \phi_e + \epsilon_r \frac{\partial}{\partial \overline{x}} \left( \epsilon_r^{-1} \frac{\partial}{\partial \overline{x}} \phi_e \right) + \frac{\partial^2}{\partial \overline{y}^2} \phi_e + \epsilon_r \phi_e = 0 \tag{2.9}$$

$$\frac{\partial^2}{\partial \overline{z}^2} \phi_h + \frac{\partial^2}{\partial \overline{x}^2} \phi_h + \epsilon_r \frac{\partial}{\partial \overline{y}} \left( \epsilon_r^{-1} \frac{\partial}{\partial \overline{y}} \phi_h \right) + \epsilon_r \phi_h = 0 \tag{2.10}$$

Both partial differential equations are of the Sturm-Liouville type. They allow to take into account the field behavior at steps of dielectric constants in a simple way. This formulation is particularly advantageous because it is self-adjoint [6].

## *2.2 Discretization*

In the Method of Lines we discretize the equations, but not completely as in finite difference methods. We discretize only as long as necessary. If we discretize in $x$ and $y$ directions, ordinary differential equations are derived from the partial differential equations. Then from these equations we obtain analytical solutions on discretization lines in $z$ direction, the main direction of propagation. From the fact of the analytical solutions on discretization lines the method has its name. Figure 2.2 shows the principle of the discretization. The figure shows that two separate line systems are used for $\phi_e$ and $\phi_h$. There are several reasons for this. One of them are the boundary conditions at the walls which are dual to each other for the two potentials. The shifting of the two line systems has still more advantages:

- the continuity conditions on permittivity steps are fulfilled very easily
- it reduces the discretization error in the case of the vector algorithm
- it results in an easy quantitative description

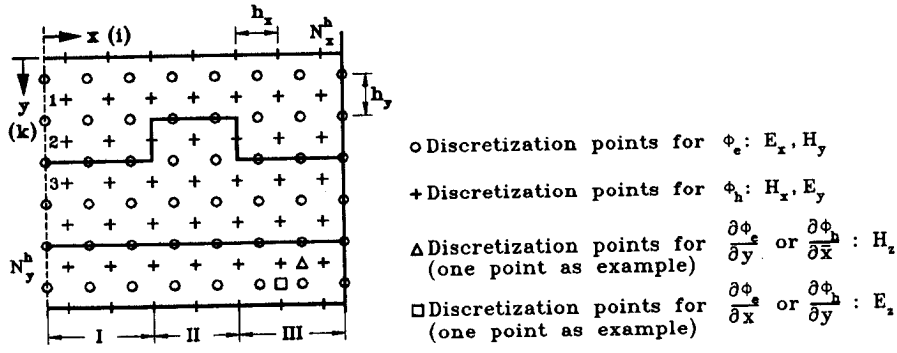


**Figure 2.2 The position of the discretization points.**

As example we choose the TM case. In the case of Fig. 2.2 the cross section could be divided into three parts. The lines for $\phi_h$ are linearly numbered by

$$n = k + (i-1)N_y^h \quad 1 \le i \le N_x^h \quad 1 \le k \le N_y^h \tag{2.11}$$

$i$ and $k$ mark the position of a line in $x$ and $y$ direction respectively. The potentials on that lines are collected in a vector $\hat{\boldsymbol{\phi}}$ of the length $N_x^h N_y^h$. In a general cross section each column of discretization points marked by $i$ has a different permittivity distribution

$$\epsilon_{rh}^i = \epsilon_{rh}^i(y_{hk}) \tag{2.12}$$

The discrete permittivities in a column $i$ are collected in a diagonal matrix $\boldsymbol{\epsilon}_{rh}^i$, where

$$\boldsymbol{\epsilon}_{rh}^i = \mathrm{diag}(\epsilon_{rh}^i(y_{hk})) \qquad k = 1, 2, ..., N_y^h \tag{2.13}$$

In the case where an interface between two different regions is part of the column, arithmetic mean values of the two permittivities besides the interface have to be introduced in this matrix as will be shown in section 2.4. The matrices $\boldsymbol{\epsilon}_{rh}^i$ for all $i$ form the diagonal matrix

$$\hat{\boldsymbol{\epsilon}}_{rh} = \mathrm{Diag}(\boldsymbol{\epsilon}_{rh}^i) \qquad i = 1, 2, ..., N_x^h \tag{2.14}$$

of permittivities for the whole cross section. For a slab guide with $\boldsymbol{\epsilon}_{rh}^i = \boldsymbol{\epsilon}_{rh}$ for all $i$ the Eq. (2.14) may be written as

$$\hat{\boldsymbol{\epsilon}}_{rh} = \boldsymbol{I}_x^h \otimes \boldsymbol{\epsilon}_{rh} \tag{2.15}$$

where $\otimes$ denotes the Kronecker product and $\boldsymbol{I}_x^h$ is the identity matrix of the order $N_x^h$.

The first order partial differential quotients are approximated by the potential differences of neighbored lines and are valid between the lines. For each column (or for every $x_{hi}$) therefore we may write a vector with the first derivatives at points $y_{h,k-\frac{1}{2}} = (k-\frac{1}{2})h_y$, $k = 1, 2, ..., N_y^h + 1$

$$h_y \frac{\partial \phi_h(x_{hi})}{\partial y} \longrightarrow \underbrace{\begin{bmatrix} -1 & & & \\ 1 & \ddots & & \\ & \ddots & -1 & \\ & & 1 & \end{bmatrix}}_{\boldsymbol{D}_y} \begin{bmatrix} \phi_{ho}^i & \phi_{h1}^i & \cdots & \phi_{hN_y^h}^i \end{bmatrix} \begin{matrix} \\ \\ \\ \\ \phi_{hN_y^h+1}^i \end{matrix} \longrightarrow \underbrace{\begin{bmatrix} a_1 & -b_1 & -c_1 & & \\ -1 & 1 & & & \\ & \ddots & \ddots & & \\ & & & -1 & 1 \\ & & c_N & b_N & -a_N \end{bmatrix}}_{\boldsymbol{D}_y^s} \begin{bmatrix} \phi_{h1}^i \\ \vdots \\ \phi_{hN_y^h}^i \end{bmatrix} \tag{2.16}$$

or with $\overline{h}_y = k_0 h_y$

$$\overline{h}_y \frac{\partial \phi_h^i}{\partial \overline{y}} \rightarrow \boldsymbol{D}_y^a \boldsymbol{\phi}_h^i \tag{2.17}$$

The difference operator $\boldsymbol{D}_y^a$ is obtained as a modified difference operator $\boldsymbol{D}_y$ with

$$\phi_{h0}^i = (1 - a_1)\phi_{h1}^i + b_1 \phi_{h2}^i + c_1 \phi_{h3}^i \tag{2.18}$$

$$\phi_{hN_y^h+1}^i = (1 - a_N)\phi_{hN_y^h}^i + b_N \phi_{hN_y^h-1}^i + c_N \phi_{hN_y^h-2}^i \tag{2.19}$$

where the constants $a_1, a_N, b_1, b_N, c_1, c_N$ have to be determined later in the section about the absorbing boundary conditions. The interpretation of the Eqs. (2.18) and (2.19) is as follows: the field outside the calculation window (linearly) depends only on the field inside the window, because we have sources only inside the window.

The difference expressions for the second order partial differential quotients may now be given as

$$\overline{h}_y^2 \frac{\partial^2 \phi_h^i}{\partial \overline{y}^2} \rightarrow -\boldsymbol{D}_y^t \boldsymbol{D}_y^a \boldsymbol{\phi}_h^i = -\boldsymbol{P}_y \boldsymbol{\phi}_h^i \tag{2.20}$$

where superscript $t$ means transpose. For our Sturm-Liouville partial differential equation (2.10) we need the difference operator for the special Sturm-Liouville term. We obtain

$$\overline{h}_y^2 \epsilon_r \frac{\partial}{\partial \overline{y}} \left( \epsilon_r^{-1} \frac{\partial \phi_h^i}{\partial \overline{y}} \right) \rightarrow -\boldsymbol{\epsilon}_{rh}^i \boldsymbol{D}_y^t (\boldsymbol{\epsilon}_{rhe}^i)^{-1} \boldsymbol{D}_y^a \boldsymbol{\phi}_h^i = -\boldsymbol{P}_{yh}^i \boldsymbol{\phi}_h^i \tag{2.21}$$

Note that the diagonal permittivity matrix between the difference operators is different from $\boldsymbol{\epsilon}_{rh}^i$. $\boldsymbol{\epsilon}_{rhe}^i$ at the discretization points $\square$ (see Fig. 2.2) is given by

$$\boldsymbol{\epsilon}_{rhe}^i = \mathrm{diag}\left( \epsilon_{rh}^i (y_{h,k-\frac{1}{2}}) \right) \qquad k = 1, 2, ..., N_y^h + 1 \tag{2.22}$$

and has one component more in the diagonal as $\boldsymbol{\epsilon}_{rh}$. As will be shown later, the value for $\epsilon_{rh}$ in this matrix at a point with permittivity step has to be chosen as arithmetic mean value of the two permittivities on both sides of the step.

Now we construct the difference operator $\hat{\boldsymbol{P}}_{yh}$ for the complete vector $\hat{\boldsymbol{\phi}}_h$:

$$\hat{\boldsymbol{P}}_{yh} = \mathrm{Diag}(\boldsymbol{P}_{yh}^i) \qquad i = 1, 2 ... N_x^h \tag{2.23}$$

which also may be written in the following form

$$\hat{\boldsymbol{P}}_{yh} = \hat{\boldsymbol{\epsilon}}_{rh}\, \hat{\boldsymbol{D}}_y^t\, \hat{\boldsymbol{\epsilon}}_{rhe}\, \hat{\boldsymbol{D}}_y^a$$

with

$$\hat{\boldsymbol{D}}_y^t = \boldsymbol{I}_x^h \otimes \boldsymbol{D}_y^t \qquad \hat{\boldsymbol{D}}_y^a = \boldsymbol{I}_x^h \otimes \boldsymbol{D}_y^a$$

For a slab guide with $\boldsymbol{P}_{yh}^i = \boldsymbol{P}_{yh}$ for all $i$ Eq. (2.23) may be written as

$$\hat{\boldsymbol{P}}_{yh} = \boldsymbol{I}_x^h \otimes \boldsymbol{P}_{yh} \tag{2.24}$$

The difference operators for the partial derivatives in $x$ direction may be written as follows

$$\hat{\boldsymbol{P}}_{xh} = \boldsymbol{P}_{xh} \otimes \boldsymbol{I}_y^h \tag{2.25}$$

with

$$\boldsymbol{P}_{xh} = \boldsymbol{D}_x^a \boldsymbol{D}_x^t \tag{2.26}$$

or

$$\hat{\boldsymbol{P}}_{xh} = \mathrm{Diag}(\boldsymbol{P}_{xh}^l \otimes \boldsymbol{I}_y^{hl}) \qquad l = 1, ..., L \quad (L = \text{number of layers}) \tag{2.27}$$

in the case where different absorbing boundary conditions are used in the different layers. $\boldsymbol{I}_y^l$ is the identity matrix of the order of the number of discretization points in $y$ direction in the layer.

Now the discretized wave equation reads as follows

$$\frac{d^2}{d\bar{z}^2}\hat{\boldsymbol{\phi}}_h - \bar{h}_x^{-2}\, \hat{\boldsymbol{P}}_{xh}\, \hat{\boldsymbol{\phi}}_h - \bar{h}_y^{-2}\, \hat{\boldsymbol{P}}_{yh}\, \hat{\boldsymbol{\phi}}_h + \hat{\boldsymbol{\epsilon}}_{rh}\, \hat{\boldsymbol{\phi}}_h = \boldsymbol{0} \tag{2.28}$$

In the quasi TE case the discretization can be done in a dual way that means the sequence of the difference operators $\boldsymbol{D}^t$ and $\boldsymbol{D}^a$ changes. Because we have now a Sturm-Liouville differential quotient according to the $x$ direction the discretization of the permittivity profile should be performed in such a way that the discretized profile could be combined with the differential operators in $x$ direction. But this is not a necessary condition. Sometimes it may be practical to combine one part of the permittivity with the differential operator for the $x$ direction and the other part with that for the $y$ direction. Especially for the medium with

$$\epsilon_r = \epsilon_{r_1}(x) + \epsilon_{r_2}(y) \tag{2.29}$$

the first term should be combined with $\boldsymbol{P}_x$ and the second term with $\boldsymbol{P}_y$. This allows a decoupled transformation for both directions with much smaller numerical effort as will be shown in the next section.

Finally it should be mentioned that metal strips may be incorporated in the analysis. If they are ideal, this can be done in the well known way for the construction of the difference matrices for the Dirichlet- or Neumann condition, respectively. But now the conditions have to be incorporated in the middle of these matrices. Not ideal metal strips with finite thickness may be handled as dielectric with complex permittivity [5].

### *2.3 Transformation for Diagonalization and Solution*

Because the matrices $\hat{\boldsymbol{P}}_x$ and $\hat{\boldsymbol{P}}_y$ in Eq. (2.28) are not diagonal the potentials are coupled with each other and the wave equation cannot be solved in this form. For diagonalization we use a transformation in two steps. In the first step we diagonalize the matrix $\hat{\boldsymbol{P}}_y$. This will be done by the transformation of the potential

$$\hat{\boldsymbol{\phi}} = \hat{\mathbf{T}}_y \overline{\hat{\boldsymbol{\phi}}} \tag{2.30}$$

where

$$\hat{\boldsymbol{T}}_y^{-1} \overline{\hat{\boldsymbol{P}}}_y^{\epsilon} \hat{\boldsymbol{T}}_y = \overline{\hat{\boldsymbol{\lambda}}}_y^2 \tag{2.31}$$

and

$$\overline{\hat{\boldsymbol{P}}}_y^{\epsilon} = \overline{h}_y^{-2} \hat{\boldsymbol{P}}_y - \hat{\boldsymbol{\epsilon}}_{rh}$$

Because $\hat{\boldsymbol{P}}_y^{\epsilon}$ is block diagonal, the solution of (2.31) is also block diagonal

$$\overline{\hat{\boldsymbol{\lambda}}}_y^2 = \mathrm{Diag}(\overline{\boldsymbol{\lambda}}_i^2) \tag{2.32}$$

$$\hat{\boldsymbol{T}}_y = \mathrm{Diag}(\boldsymbol{T}_{yi}) \tag{2.33}$$

where

$$\mathbf{T}_{yi}^{-1} \overline{\boldsymbol{P}}_{yi}^{\epsilon} \boldsymbol{T}_{yi} = \overline{\boldsymbol{\lambda}}_i^2 \qquad i = 1, 2, ..., N_x \tag{2.34}$$

and

$$\overline{\boldsymbol{P}}_{yi}^{\epsilon} = \overline{h}_y^{-2} \boldsymbol{P}_y^i - \boldsymbol{\epsilon}_{rh}^i$$

Therefore in a general case $N_x$ eigenvalue problems of the order $N_y$ must be solved. But in most cases only some different matrices $\mathbf{P}_{yi}$

exist. In the case of the cross section in Fig. 2.2 in each of the regions $I, II$ or $III$ we have only one type of $\boldsymbol{P}_y$. In addition we have different types for the columns which separate the regions.

The second transformation is defined by

$$\hat{\hat{\underline{\phi}}} = \hat{\boldsymbol{T}}_x \hat{\hat{\underline{\phi}}} \tag{2.35}$$

and

$$\hat{\boldsymbol{T}}_x^{-1}(\bar{h}_x^{-2}\hat{\boldsymbol{T}}_y^{-1}\hat{\boldsymbol{P}}_x\hat{\boldsymbol{T}}_y + \hat{\bar{\boldsymbol{\lambda}}}_y^2)\hat{\boldsymbol{T}}_x = \hat{\bar{\boldsymbol{\lambda}}}^2 \tag{2.36}$$

In the case where Eq. (2.24) or Eq. (2.29) is valid, also Eq. (2.36) becomes simpler:

$$\hat{\bar{\boldsymbol{\lambda}}}_x^2 + \hat{\bar{\boldsymbol{\lambda}}}_y^2 = \hat{\bar{\boldsymbol{\lambda}}}^2 \tag{2.37}$$

with

$$\begin{aligned} \hat{\bar{\boldsymbol{\lambda}}}_x^2 &= \bar{\boldsymbol{\lambda}}_x^2 \otimes \boldsymbol{I}_y \\ \hat{\boldsymbol{T}}_x &= \boldsymbol{T}_x \otimes \boldsymbol{I}_y \\ \bar{h}_x^{-2}\boldsymbol{T}_x^{-1}\boldsymbol{P}_x\boldsymbol{T}_x &= \bar{\boldsymbol{\lambda}}_x^2 \end{aligned} \tag{2.38}$$

or

$$\bar{h}_x^{-2}\boldsymbol{T}_x^{-1}\boldsymbol{P}_x^{\epsilon}\boldsymbol{T}_x = \bar{\boldsymbol{\lambda}}_x^2$$

respectively. $\boldsymbol{P}_x^{\epsilon}$ is constructed in an analog manner from $\boldsymbol{P}_x$ and $\boldsymbol{\epsilon}_{r1}(x)$ as $\boldsymbol{P}_y^{\epsilon}$ from $\boldsymbol{P}_y$ and $\boldsymbol{\epsilon}_{r2}(y)$. This last result is the same as in [16] for the basic medium.

It is clear that the diagonalization can also be done in one step.

With $\hat{\bar{\boldsymbol{\lambda}}}^2$ from Eq. (2.36) or (2.37) (or from the one step diagonalization solution) the wave equation reads

$$\frac{d^2}{dz^2}\hat{\hat{\underline{\phi}}} - \hat{\bar{\boldsymbol{\lambda}}}^2\hat{\hat{\underline{\phi}}} = 0 \tag{2.39}$$

with the solution

$$\hat{\hat{\underline{\phi}}}(z) = e^{-\boldsymbol{\Gamma}\bar{z}}\hat{\hat{\underline{\phi}}}(0) \tag{2.40}$$

for propagation in $+z$ direction and where $\boldsymbol{\Gamma} = \hat{\bar{\boldsymbol{\lambda}}}$ is the diagonal matrix of normalized propagation constants. To obtain the field (or the

potentials) in the original domain inverse transform according to Eqs. (2.30) and (2.35) must be performed.

## *2.4 Interface Conditions at Permittivity Steps*

As described in the section 2.2 we put the discretization points for $\phi_h$ on the interface line at permittivity steps in horizontal or $x$ direction (interface line in vertical direction) and we put the discretization points for $\phi_e$ on the interface line at permittivity steps in vertical or $y$ direction (interface line in horizontal direction). Therefore in the first case the interface line is lying between the $\phi_e$ points and in the second case between the $\phi_h$ points. This we have done according to the behavior of the potentials at the interface. Because of the continuity of the tangential $E$ field and the normal $D$ field components at $u = u_t$, we have to fulfill the conditions (see Figure 2.3)

$$\phi_{\alpha t}^1 = \phi_{\alpha t}^2 \tag{2.41}$$

$$\frac{1}{\epsilon_{r1}} \frac{\partial \phi_\alpha^1}{\partial u} = \frac{1}{\epsilon_{r2}} \frac{\partial \phi_\alpha^2}{\partial u} \tag{2.42}$$

where

$$\begin{aligned} &\text{for } \alpha \equiv e \quad \text{then } u \equiv x, \quad m = i \\ &\text{for } \alpha \equiv h \quad \text{then} u \equiv y, \quad m = k \end{aligned} \tag{2.43}$$

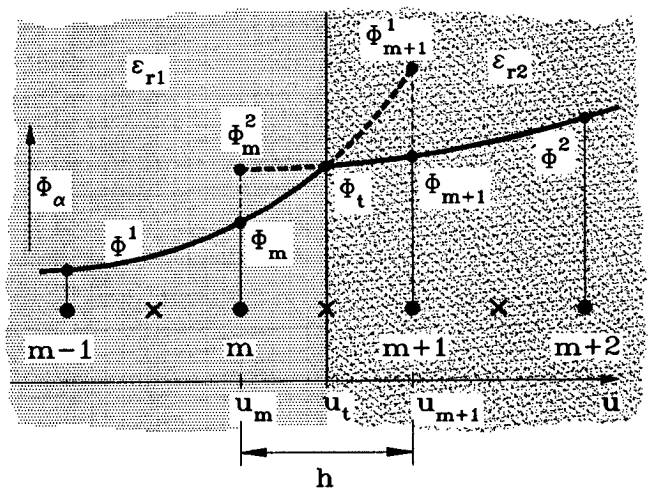


**Figure 2.3 Behavior of $\phi_\alpha$ at an abrupt transition from $\epsilon_{r1}$ to $\epsilon_{r2}$.**

Consequently, in the figure the curve for $\phi_\alpha$ (The subscript $\alpha$ is omitted in the figure and in the following for simplicity) is drawn with a break at $u = u_t$. For the definition of the auxiliary quantities $\phi^1_{m+1}$ and $\phi^2_m$ the dashed curves are drawn without any break. These auxiliary quantities are necessary to compute the second derivative on the points $m$ and $m+1$ (lines in $z$ direction). With the Taylor series up to the linear term, applied on the interface point $u_t$ it is found

$$\phi^1(u_{m+1}) = \phi^1_{m+1} \approx \phi_t + \frac{h}{2}\frac{\partial \phi^1}{\partial u}$$

$$\phi^2(u_m) = \phi^2_m \approx \phi_t - \frac{h}{2}\frac{\partial \phi^2}{\partial u}$$

$$\phi(u_{m+1}) = \phi_{m+1} \approx \phi_t + \frac{h}{2}\frac{\partial \phi^2}{\partial u}$$

$$\phi(u_m) = \phi_m \approx \phi_t - \frac{h}{2}\frac{\partial \phi}{\partial u}$$

The condition in Eq. (2.41) is fulfilled immediately by these equations. With Eq. (2.42) we find for the derivatives on both sides of the interface

$$h\frac{\partial \phi^1}{\partial u} = \frac{\epsilon_{r1}}{\epsilon_{rt}}(\phi_{m+1} - \phi_m) \tag{2.44}$$

$$h\frac{\partial \phi^2}{\partial u} = \frac{\epsilon_{r2}}{\epsilon_{rt}}(\phi_{m+1} - \phi_m) \tag{2.45}$$

where

$$\epsilon_{rt} = \frac{\epsilon_{r1} + \epsilon_{r2}}{2} + [p(\epsilon_{r1} - \epsilon_{r2})] \tag{2.46}$$

The term in the brackets must be added if the interface is moved in $u$ direction by $ph(-0.5 \leq p \leq 0.5)$. Now also the special second order derivatives in the Sturm-Liouville wave equation can be discretized on points $m$ and $m+1$.

$$h^2\epsilon_r \frac{\partial}{\partial u}\left(\frac{1}{\epsilon_r}\frac{\partial \phi}{\partial u}\right)_m \approx \frac{\epsilon_{r1}}{\epsilon_{rt}}(\phi_{m+1} - \phi_m) - (\phi_m - \phi_{m-1}) \tag{2.47}$$

$$h^2\epsilon_r \frac{\partial}{\partial u}\left(\frac{1}{\epsilon_r}\frac{\partial \phi}{\partial u}\right)_{(m+1)} \approx (\phi_{m+2} - \phi_{m+1}) - \frac{\epsilon_{r2}}{\epsilon_{rt}}(\phi_{m+1} - \phi_m) \tag{2.48}$$

We get the same results if we fill the place for the point at the interface in the diagonal matrix $\boldsymbol{\epsilon}_r$ which is positioned between the difference operators $\boldsymbol{D}^t$ and $\boldsymbol{D}^a$ ($\boldsymbol{\epsilon}_{rhe}$ in Eq. (2.21)) of the special difference operator $\boldsymbol{P}$ with the value $\epsilon_{rt}$. We can understand this result easily. The first order derivative is obtained at points between the discretization points. Therefore for the derivatives which we obtain on the transition the corresponding $\epsilon_r$ value must be chosen. Because of the step the arithmetic mean value of the two values beside the interface must be used.

The same is true for the places in the diagonal matrices $\boldsymbol{\epsilon}_r$ belonging to discretization points on permittivity interfaces ( $\boldsymbol{\epsilon}^i_{rh}$ on vertical interfaces, $\boldsymbol{\epsilon}^i_{re}$ on horizontal interfaces). Then also the interface conditions for the other field components are fulfilled as can be seen from Eq. (2.8). Improved approximations for interface conditions are described in [23].

## *2.5 Two Step Algorithm*

This full wave algorithm has many advantages as demonstrated. The disadvantage is that in the 3D case the numerical effort is very high. If the number of discretization points is $N_x$ and $N_y$ in the two directions respectively, we have matrices of the order $N_x$ times $N_y$, which are complex in general. Therefore we also have developed an alternative algorithm, which is a split-step procedure. Split-step procedures are also used in FFT-BPM and in FD-BPM. But there are significant differences. The main difference is that we use a multilayered reference medium instead of a homogeneous one. This multilayered reference medium is nearly identical with the waveguide cross section. In case of e.g. a rib guide shown in the Fig. 2.4, the reference guide differs from the original structure in the layer for the rib only.

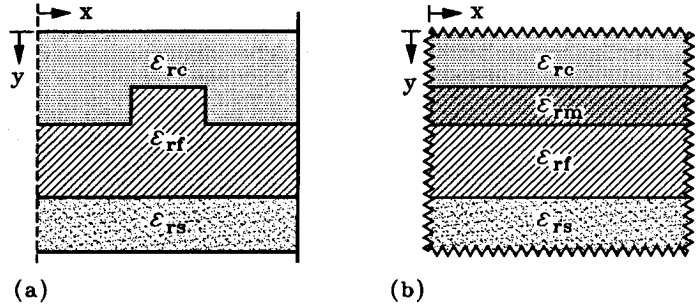


(a) (b)

**Figure 2.4 Reference medium (b) for a rib waveguide (a).**

Thus the reference medium has the correct refractive index in the region with the main field of our wave. The correction is only necessary in regions of the cross sections where the field intensity is small.

In the general case the reference medium has the permittivity

$$\epsilon_R = \epsilon_{r_1}(x) + \epsilon_{r_2}(y) \tag{2.49}$$

Thus the reference medium is a double layered structure. The propagation in this reference medium is described by (see section 2.3)

$$\hat{\boldsymbol{\phi}}_o(z) = \hat{\boldsymbol{T}}\ e^{-\boldsymbol{\Gamma}\overline{z}}\ \hat{\boldsymbol{T}}^{-1}\ \hat{\boldsymbol{\phi}}_0\ (0) \tag{2.50}$$

with (Eqs. (2.33) and (2.37))

$$\hat{\boldsymbol{T}} = \boldsymbol{T}_x \otimes \boldsymbol{T}_y \tag{2.51}$$

and

$$\boldsymbol{\Gamma}^2 = \overline{\boldsymbol{\lambda}}_x^2 \otimes \boldsymbol{I}_y + \boldsymbol{I}_x \overline{\boldsymbol{\lambda}}_y^2 \tag{2.52}$$

Thus the propagation of the field in the reference medium is again described by eigenmodes. But now a separate diagonalization of the difference matrices with respect to the coordinate directions is possible. The two eigenvalue problems for $\boldsymbol{P}_x^{\epsilon}$ and $\boldsymbol{P}_y^{\epsilon}$ which have to be solved are only of the order $N_x$ and $N_y$ respectively.

To obtain the propagation behavior in the original structure we make an ansatz by the product of the solution in the reference medium and a correction factor

$$\phi(x,y,z) = \phi_o(x,y,z)e^{-jQ(x,y,z)} \tag{2.53}$$

or in discretized form

$$\hat{\boldsymbol{\phi}} = e^{-j\hat{\mathbf{Q}}}\hat{\boldsymbol{\phi}}_0 \tag{2.54}$$

Introducing this ansatz into the wave equation and neglecting the second order derivative of $\boldsymbol{Q}$ we obtain a specific formula for "phase" correction

$$\left(\frac{d\hat{\mathbf{Q}}}{d\overline{z}}\right)^2 - 2j\,\boldsymbol{\phi}_m^{-1}\ \hat{\boldsymbol{T}}\ \boldsymbol{\Gamma}\ \hat{\boldsymbol{T}}^{-1}\ \hat{\boldsymbol{\phi}}_o \cdot \frac{d\hat{\mathbf{Q}}}{d\overline{z}} - \hat{\boldsymbol{\epsilon}}_{rd} = 0 \tag{2.55}$$

where

$$\hat{\epsilon}_{rd} = \hat{\epsilon}_r - \hat{\epsilon}_R \tag{2.56}$$

and $\phi_m$ is the diagonal matrix obtained from the vector $\hat{\phi}_0$

$$\phi_m = \mathrm{diag}((\hat{\phi}_0)_n) \tag{2.57}$$

For a homogeneous reference medium with $\Gamma = jn_o\hat{I}$ the above equation reduces to the well known formula

$$\frac{d\hat{Q}}{d\bar{z}} = \hat{n} - \hat{n}_o \tag{2.58}$$

where $\hat{n}^2 = \epsilon_r$ and $\hat{n}_o^2 = \epsilon_{ro}$. In our case $Q$ is complex. Therefore also an amplitude correction is performed.

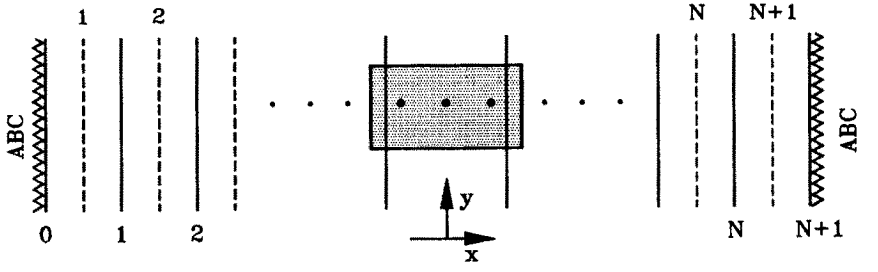


**Figure 3.1 Absorbing boundary conditions on the left and on the right side of a waveguide.**

## 3. Absorbing Boundary Conditions (ABC)

### *3.1 Factorization of the Helmholtz Equation and Approximation*

In inhomogeneous waveguide structures a part of the field of a propagating wave is scattered. This scattered field propagates to the walls and must be absorbed there to avoid reflections. In the MoL-BPM absorbing boundary conditions (ABC) as described in [9] are introduced for this task. The ABCs are obtained by factorization of the wave equation. We will demonstrate the procedure for the $x$ direction (see Fig. 3.1). Using the operator $L$ where

$$L = \frac{\partial^2}{\partial \overline{x}^2} + \frac{\partial^2}{\partial \overline{y}^2} + \frac{\partial^2}{\partial \overline{z}^2} + \epsilon_r = D_{\overline{x}}^2 + D_{\overline{y}}^2 + D_{\overline{z}}^2 + \epsilon_r \tag{3.1}$$

we write instead of the wave equation

$$L\phi = L^+ L^- \phi = 0 \tag{3.2}$$

with solutions for propagating fields in $+x$ and $-x$ direction two separate equations

$$L^+\phi = 0 \quad \text{and} \quad L^-\phi = 0 \tag{3.3}$$

where

$$L^+\phi = \left(D_{\overline{x}} + j\sqrt{\epsilon_r}\sqrt{1+S^2}\right)\phi = 0 \tag{3.4}$$

$$L^-\phi = \left(D_{\overline{x}} - j\sqrt{\epsilon_r}\sqrt{1+S^2}\right)\phi = 0 \tag{3.5}$$

$$S^2 = \epsilon_r^{-1}\left(D_{\overline{y}}^2 + D_{\overline{z}}^2\right) \tag{3.6}$$

The first one describes wave propagation only in $+x$ direction and the second one only in $-x$ direction. The scattered field from the guide in Fig. 3.1 propagates on the right side in $+x$ direction and on the left side in $-x$ direction. On both sides only outgoing waves are allowed. Therefore on the right side the field will be described by Eq. (3.4) only and on the left side by Eq. (3.5) only. The ABCs will be obtained now from these two equations for the right and left boundary, respectively. The main problem in Eqs. (3.4) and (3.5) is the square root with differential operators in the radicant. Therefore $L^+$ and $L^-$ are nonlocal pseudodifferential operators and a direct numerical implementation is not possible. The usual way [9] to overcome this problem is the following Padé approximation by the rational function

$$\sqrt{1+S^2} \approx \frac{p_0 + p_2 S^2}{q_0 + q_2 S^2} \qquad |S^2| < 1 \tag{3.7}$$

With this approximation we can write for the Eqs. (3.4) and (3.5)

$$\left\{\mp j\left[q_0 + q_2\epsilon_r^{-1}\left(D_{\overline{y}}^2 + D_{\overline{z}}^2\right)\right] D_{\overline{x}} + \sqrt{\epsilon_r}\left[p_0 + p_2\epsilon_r^{-1}\left(D_{\overline{y}}^2 + D_{\overline{z}}^2\right)\right]\right\}\phi = 0$$

Introducing

$$D_{\bar{y}}^2 + D_{\bar{z}}^2 = -\epsilon_r - D_{\bar{x}}^2$$

from the wave equation, we obtain

$$\left\{\epsilon_r^{-1} D_{\bar{x}}^2 \pm j\left[\frac{q_0}{p_2} - \frac{q_2}{p_2}\left(1 + \epsilon_r^{-1} D_{\bar{x}}^2\right)\right] \epsilon_r^{-\frac{1}{2}} D_{\bar{x}} + \left(1 - \frac{p_0}{p_2}\right)\right\} \phi = 0 \tag{3.8}$$

Discretizing this equation on line 1 with the minus sign and on line N with the plus sign by using Taylor series at this lines to obtain the potentials on the neighborhood lines gives

$$\begin{Bmatrix} \phi_o \\ \\ \phi_{N+1} \end{Bmatrix} = \frac{2p_2 - \frac{1}{2}\bar{n}_a(1-q_2) + 3q_2\bar{n}_a^{-1} + (p_2 - p_0)\bar{n}_a^2}{p_2 + \frac{1}{3}\bar{n}_a(1-q_2) + q_2\bar{n}_a^{-1}} \begin{Bmatrix} \phi_1 \\ \\ \phi_N \end{Bmatrix}$$

$$- \frac{p_2 - \bar{n}_a(1-q_2) + 3q_2\bar{n}_a^{-1}}{p_2 + \frac{1}{3}\bar{n}_a(1-q_2) + q_2\bar{n}_a^{-1}} \begin{Bmatrix} \phi_2 \\ \\ \phi_{N-1} \end{Bmatrix}$$

$$- \frac{\frac{1}{6}\bar{n}_a(1-q_2) - q_2\bar{n}_a^{-1}}{p_2 + \frac{1}{3}\bar{n}_a(1-q_2) + q_2\bar{n}_a^{-1}} \begin{Bmatrix} \phi_3 \\ \\ \phi_{N-2} \end{Bmatrix}$$

with the abbreviation $\bar{n}_a = j\bar{h}\sqrt{\epsilon_r}$ and where without loss of generality $q_0 = 1$ was introduced. From this equation the coefficients $a_1, a_N, b_1, b_N$ and $c_1, c_N$ are found.

$$a_{1(N)} = 1 - \frac{2p_2 - \frac{1}{2}\bar{n}_a(1-q_2) + 3q_2\bar{n}_a^{-1} + (p_2 - p_0)\bar{n}_a^2}{p_2 + \frac{1}{3}\bar{n}_a(1-q_2) + q_2\bar{n}_a^{-1}} \tag{3.9}$$

$$b_{1(N)} = - \frac{p_2 - \bar{n}_a(1-q_2) + 3q_2\bar{n}_a^{-1}}{p_2 + \frac{1}{3}\bar{n}_a(1-q_2) + q_2\bar{n}_a^{-1}} \tag{3.10}$$

$$c_{1(N)} = - \frac{\frac{1}{6}\bar{n}_a(1-q_2) - q_2\bar{n}_a^{-1}}{p_2 + \frac{1}{3}\bar{n}_a(1-q_2) + q_2\bar{n}_a^{-1}} \tag{3.11}$$

It should be mentioned that the parameters $\epsilon_r, p_0, p_2$ and $q_2$ can be different on both sides of the waveguide. Therefore the absorbing boundary conditions on both sides of the waveguide are different in general. The expansion coefficients are chosen from the three angles

$\Theta_1, \Theta_2$ and $\Theta_3$ with total absorption. At other angles the numerical implementation is not exact. The reflection coefficient at the boundary is given by [10]

$$r = \frac{\cos\Theta - q_2 \cos\Theta \sin^2\Theta - p_0 + p_2 \sin^2\Theta}{\cos\Theta - q_2 \cos\Theta \sin^2\Theta + p_0 - p_2 \sin^2\Theta} \tag{3.12}$$

In Fig. 3.2 this reflection coefficient $r$ is shown depending on the angle of incidence $\Theta$ for different approximations and various choices of absorbing angles $\Theta_i$.

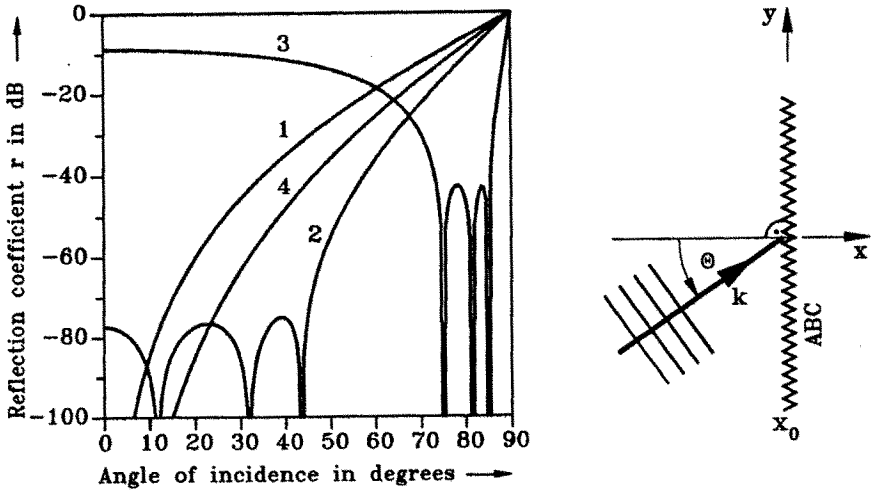


**Figure 3.2 Reflection coefficient $r$ at the boundary depending on the angle of incidence $\Theta$.**

Therefore with $r = 0$ for three chosen angles $\Theta_1, \Theta_2$ and $\Theta_3$ we obtain the coefficients from

$$\begin{bmatrix} 1 & -\sin^2\Theta_1 & \cos\Theta_1 \sin^2\Theta_1 \\ 1 & -\sin^2\Theta_2 & \cos\Theta_2 \sin^2\Theta_2 \\ 1 & -\sin^2\Theta_3 & \cos\Theta_3 \sin^2\Theta_3 \end{bmatrix} \begin{bmatrix} p_0 \\ p_2 \\ q_2 \end{bmatrix} = \begin{bmatrix} \cos\Theta_1 \\ \cos\Theta_2 \\ \cos\Theta_3 \end{bmatrix}$$

with the solution

$$\begin{aligned} q_2 =& (1 + \cos\Theta_1 \cos\Theta_2 + \cos\Theta_1 \cos\Theta_3 + \cos\Theta_2 \cos\Theta_3)^{-1} \\ p_0 =& (\cos\Theta_1 + \cos\Theta_2 + \cos\Theta_3 + \cos\Theta_1 \cos\Theta_2 \cos\Theta_3) q_2 \\ p_2 =& (\cos\Theta_1 + \cos\Theta_2 + \cos\Theta_3) q_2 \end{aligned} \tag{3.13}$$

which may be obtained with e.g. MAPLE. The angles of total absorption can be chosen in such a way that in a specified region equiripple reflection behavior is obtained.

### *3.2 Other Approximations*

In the case $q_2 = 0$ (polynomial approximation) and two angles $\Theta_1$ and $\Theta_2$ of total absorption we obtain the solution

$$p_0 = \frac{1 + \cos\Theta_1 \cos\Theta_2}{\cos\Theta_1 + \cos\Theta_2} \qquad p_2 = \frac{1}{\cos\Theta_1 + \cos\Theta_2} \tag{3.14}$$

By an alternative discretization [15] the following coefficients are obtained

$$a_{1(\mathrm{N})} = 1 - 2\frac{2p_2 + (p_2 - p_0)\overline{n}_a^2}{2p_2 + \overline{n}_a} \qquad b_{1(\mathrm{N})} = -\frac{2p_2 - \overline{n}_a}{2p_2 + \overline{n}_a} \qquad c_{1(\mathrm{N})} = 0 \tag{3.15}$$

To obtain optimal absorption in the vicinity of $\Theta = 0$ we also can use a Taylor expansion for the square root of fourth order

$$\sqrt{1 + S^2} = 1 + \frac{1}{2}S^2 - \frac{1}{8}S^4 \tag{3.16}$$

The corresponding operator equation analog to Eq. (3.8) can be factorized in the following form

$$\{(D_{\overline{x}} \pm j\sqrt{\epsilon_r})^3 (D_{\overline{x}} \pm j3\sqrt{\epsilon_r})\}\phi = 0 \tag{3.17}$$

The first factor produces a third order reflection zero at $\Theta = 0$. Therefore an improved behavior of $r$ is obtained (see curve 4 in Fig. 3.2). For the second factor a wave with a real angle of incidence does not exist. Therefore some care is necessary for using this approximation. For discretization of this equation a potential at one more discretization point as for Eq. (3.8) is necessary.

# 4. Analysis of Waveguide Bends, Waveguide Steps and Bragg Gratings

In this chapter we will give the basic equations for the modeling of waveguide bends, e.g. the S-bend with offsets [24] in Fig. 4.1.

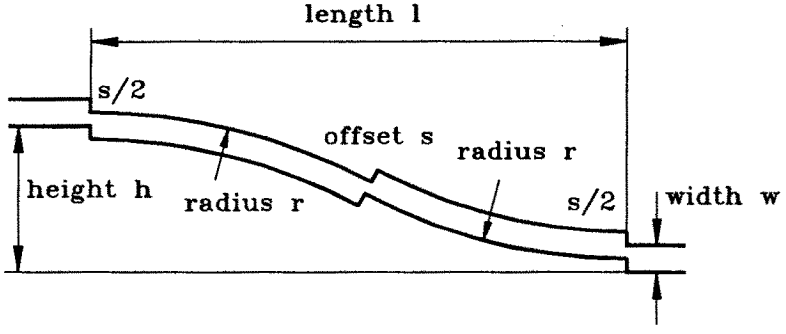


**Figure 4.1 Optical waveguide S-bend with offsets for field matching.**

## *4.1 Waveguide bends*

We start with the bend in Fig. 4.2. We divide the bend into sectors with suitable angles $\alpha_m$. Each sector is approximated by a straight waveguide with end planes equal to the sector planes, which are not normal to the propagation direction. Therefore the propagation steps are individual on each discretization line. The basic element is shown in Fig. 4.2b.

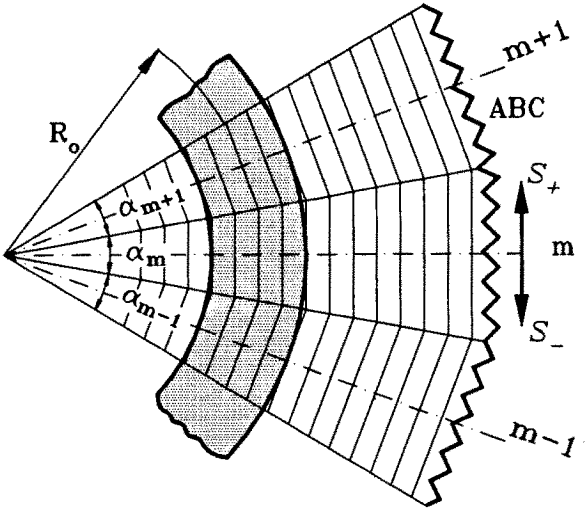


(a)

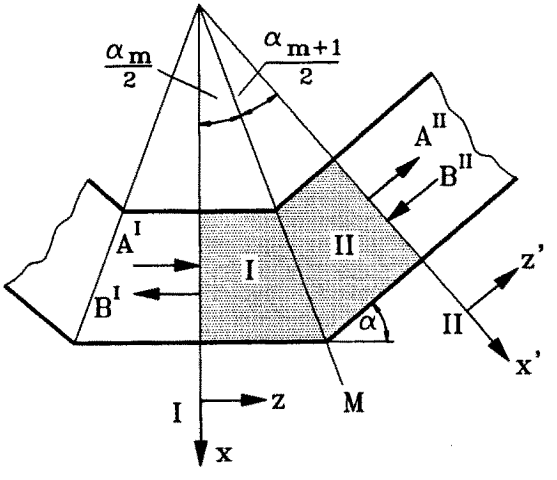


(b)

**Figure 4.2 Model of the waveguide bend (a) and its basic element (b).**

The MoL-BPM uses not only guided but also radiation modes in the structure. Therefore the fields in the two optical waveguides $I$ and $II$ including reflections are given by

$$\overline{\boldsymbol{\phi}}^{I} = e^{-\boldsymbol{\Gamma}_I \overline{z}} \boldsymbol{A}^{I} + e^{\boldsymbol{\Gamma}_I \overline{z}} \mathbf{B}^{I} \tag{4.1}$$

$$\overline{\boldsymbol{\phi}}^{II} = e^{-\boldsymbol{\Gamma}_{II} \overline{z}'} \boldsymbol{A}^{II} + e^{\boldsymbol{\Gamma}_{II} \overline{z}'} \boldsymbol{B}^{II} \tag{4.2}$$

At all quantities a subscript $e$ or $h$ for TE or TM mode case, respectively, must be added. The components of the vectors $\mathbf{A}^I$ and $\boldsymbol{A}^{II}$ are the amplitudes of the modes in $+z$ and $+z'$ direction, the components of $\boldsymbol{B}^I$ and $\boldsymbol{B}^{II}$ are the amplitudes in $-z$ and $-z'$ direction. $\boldsymbol{\Gamma}$ is the diagonal matrix of the propagation constants (see Eq. (2.40)).

The next step is the field matching in the cross section $M$ in which each point has another distance to the reference planes $I$ and $II$. The distances are equal to the individual propagation steps $\Delta z$. The main components which have to be matched are in the

*TM case*

$$\begin{aligned} E_y &= -\epsilon_r^{-1}\left(\frac{\partial^2 \phi_h}{\partial \overline{x}^2} + \frac{\partial^2 \phi_h}{\partial \overline{z}^2}\right) = \frac{\partial}{\partial \overline{y}}\left(\epsilon_r^{-1}\frac{\partial}{\partial \overline{y}}\phi_h\right) + \phi_h \\ \eta_0 H_x &= -j\frac{\partial \phi_h}{\partial \overline{z}} \end{aligned} \tag{4.3}$$

*TE case*

$$\begin{aligned} E_x &= -\epsilon_r^{-1}\left(\frac{\partial^2 \phi_e}{\partial \overline{y}^2} + \frac{\partial^2 \phi_e}{\partial \overline{z}^2}\right) = \frac{\partial}{\partial \overline{x}}\left(\epsilon_r^{-1}\frac{\partial}{\partial \overline{x}}\phi_e\right) + \phi_e \\ \eta_0 H_y &= j\frac{\partial \phi_e}{\partial \overline{z}} \end{aligned} \tag{4.4}$$

Because the two waveguide cross sections are identical, the potential and its derivative according to $z$ and $z'$, respectively, are to be matched instead of the field components. From Eqs. (4.1) and (4.2) we obtain

$$\frac{d\bar{\boldsymbol{\phi}}^I}{d\bar{z}} = -\left(e^{-\boldsymbol{\Gamma}_I\bar{z}}\boldsymbol{\Gamma}_I\mathbf{A}^I - e^{\boldsymbol{\Gamma}_I\bar{z}}\boldsymbol{\Gamma}_I\mathbf{B}^I\right) \tag{4.5}$$

$$\frac{d\bar{\boldsymbol{\phi}}^{II}}{d\bar{z}'} = -\left(e^{-\boldsymbol{\Gamma}_{II}\bar{z}'}\boldsymbol{\Gamma}_{II}\boldsymbol{A}^{II} - e^{\boldsymbol{\Gamma}_{II}\bar{z}'}\boldsymbol{\Gamma}_{II}\boldsymbol{B}^{II}\right) \tag{4.6}$$

The matching process must be done in the original domain and yields

$$\begin{aligned} \tau_e\boldsymbol{S}_{I+}\boldsymbol{A}^I + \boldsymbol{S}_{I-}\boldsymbol{B}^I &= \boldsymbol{S}_{II-}\boldsymbol{A}^{II} + \tau_e\boldsymbol{S}_{II+}\boldsymbol{B}^{II} \\ \tau_h\boldsymbol{R}_{I+}\boldsymbol{A}^I - \boldsymbol{R}_{I-}\boldsymbol{B}^I &= \boldsymbol{R}_{II-}\boldsymbol{A}^{II} - \tau_h\boldsymbol{R}_{II+}\boldsymbol{B}^{II} \end{aligned} \tag{4.7}$$

or

$$\begin{bmatrix} \tau_e\boldsymbol{S}_{I+} & -\tau_e\boldsymbol{S}_{II+} \\ \tau_h\boldsymbol{R}_{I+} & \tau_h\boldsymbol{R}_{II+} \end{bmatrix} \begin{bmatrix} \boldsymbol{A}^I \\ \boldsymbol{B}^{II} \end{bmatrix} = \begin{bmatrix} \boldsymbol{S}_{II-} & -\boldsymbol{S}_{I-} \\ \boldsymbol{R}_{II-} & \boldsymbol{R}_{I-} \end{bmatrix} \begin{bmatrix} \boldsymbol{A}^{II} \\ \boldsymbol{B}^I \end{bmatrix} \tag{4.8}$$

with

$$(\boldsymbol{S}_\pm)_{n,n'} = (\hat{\boldsymbol{T}})_{n,n'} e^{\mp(\boldsymbol{\Gamma})_{n'}\Delta\bar{z}_n} \tag{4.9}$$

$$\Delta\bar{z}_n = \Delta z_0 + h\tan\frac{\alpha_M}{2}\ \mathrm{INT}\left(\frac{n-1}{N_y}\right)$$

$$\alpha_M = \alpha_m \text{ or } \alpha_{m+1}\text{ , respectively}$$

$$\boldsymbol{R}_\pm = \boldsymbol{S}_\pm\boldsymbol{\Gamma} \tag{4.10}$$

and

$$\tau_e = \frac{\cos(\frac{\alpha_m}{2})}{\cos(\frac{\alpha_{m+1}}{2})} \qquad \tau_h = 1 \qquad \text{for the TE case}$$

$$\tau_h = \frac{\cos(\frac{\alpha_m}{2})}{\cos(\frac{\alpha_{m+1}}{2})} \qquad \tau_e = 1 \qquad \text{for the TM case}$$

$\tau_e$ and $\tau_h$ are necessary because the two angles $\alpha_m$ and $\alpha_{m+1}$ are not equal in general. Therefore we also must distinguish between the

two regions $I$ and $II$ for $\mathbf{S}$ and $\boldsymbol{R}$. To obtain the transmitted and reflected waves for a single sharp bend we set $\mathbf{B}^{II} = \mathbf{0}$ and get

$$\begin{aligned}\boldsymbol{A}^{II} &= \left(\boldsymbol{R}_{I-}^{-1}\boldsymbol{R}_{II-} + \boldsymbol{S}_{I-}^{-1}\boldsymbol{S}_{II-}\right)^{-1}\left(\tau_h\boldsymbol{R}_{I-}^{-1}\boldsymbol{R}_{I+} + \tau_e\boldsymbol{S}_{I-}^{-1}\boldsymbol{S}_{I+}\right)\boldsymbol{A}^{I} \\ &= \boldsymbol{S}\boldsymbol{A}^{I} \end{aligned} \tag{4.11}$$

$$\begin{aligned}\boldsymbol{B}^{I} &= \left(\boldsymbol{R}_{II-}^{-1}\boldsymbol{R}_{I-} + \boldsymbol{S}_{II-}^{-1}\boldsymbol{S}_{I-}\right)^{-1}\left(\tau_h\boldsymbol{R}_{II-}^{-1}\boldsymbol{R}_{I+} - \tau_e\boldsymbol{S}_{II-}^{-1}\boldsymbol{S}_{I+}\right)\boldsymbol{A}^{I} \\ &= \boldsymbol{R}\boldsymbol{A}^{I} \end{aligned} \tag{4.12}$$

For $\boldsymbol{S}_I = \boldsymbol{S}_{II}$, that means for a constant bend radius which implies $\alpha_m = \alpha_{m+1}$, we obtain

$$\boldsymbol{A}^{II} = \frac{1}{2}\left(\boldsymbol{R}_{-}^{-1}\boldsymbol{R}_{+} + \boldsymbol{S}_{-}^{-1}\boldsymbol{S}_{+}\right)\boldsymbol{A}^{I} = \boldsymbol{S}\boldsymbol{A}^{I} \tag{4.13}$$

$$\boldsymbol{B}^{I} = \frac{1}{2}\left(\boldsymbol{R}_{-}^{-1}\boldsymbol{R}_{+} - \boldsymbol{S}_{-}^{-1}\boldsymbol{S}_{+}\right)\boldsymbol{A}^{I} = \boldsymbol{R}\boldsymbol{A}^{I} \tag{4.14}$$

Neglecting reflections, Eq. (4.11) yields a recurrence relation for the analysis of waveguide bends

$$\begin{aligned}\boldsymbol{A}_{m+1} &= \left(\boldsymbol{R}_{I-}^{-1}\boldsymbol{R}_{II-} + \boldsymbol{S}_{I-}^{-1}\boldsymbol{S}_{II-}\right)^{-1}\left(\tau_h\boldsymbol{R}_{I-}^{-1}\boldsymbol{R}_{I+} + \tau_e\boldsymbol{S}_{I-}^{-1}\boldsymbol{S}_{I+}\right)\boldsymbol{A}_m \\ &= \boldsymbol{S}_m\boldsymbol{A}_m \end{aligned} \tag{4.15}$$

where the quantities $\boldsymbol{S}$ and $\boldsymbol{R}$ in the parentheses may change from one sector to the other. To obtain the real field in a cross section, an inverse transform with $\boldsymbol{T}_e$ or $\boldsymbol{T}_h$ for the TE or TM case, respectively, must be performed.

If we rewrite Eqs. (4.8) for the case $\boldsymbol{S}_{I\pm} = \mathbf{S}_{II\pm}$, we obtain

$$\begin{bmatrix} \boldsymbol{S}_{-}^{-1}\boldsymbol{S}_{+} & \\ & \boldsymbol{R}_{-}^{-1}\boldsymbol{R}_{+} \end{bmatrix}\begin{bmatrix} \boldsymbol{I} & -\boldsymbol{I} \\ \boldsymbol{I} & \boldsymbol{I} \end{bmatrix}\begin{bmatrix} \boldsymbol{A}^{I} \\ \boldsymbol{B}^{II} \end{bmatrix} = \begin{bmatrix} \boldsymbol{I} & -\boldsymbol{I} \\ \boldsymbol{I} & \boldsymbol{I} \end{bmatrix}\begin{bmatrix} \boldsymbol{A}^{II} \\ \boldsymbol{B}^{I} \end{bmatrix} \tag{4.16}$$

For equal sectors Floquets theorem may be introduced

$$\boldsymbol{A}^{II} = \boldsymbol{A}^{I}e^{-\boldsymbol{\Gamma}_p} \qquad \boldsymbol{B}^{I} = \boldsymbol{B}^{II}e^{-\boldsymbol{\Gamma}_p} \tag{4.17}$$

with $\boldsymbol{\Gamma}_p$ as the diagonal matrix of the propagation constants for the periodic structure. Solutions are obtained from

$$\boldsymbol{S}_{-}^{-1}\boldsymbol{S}_{+}(\boldsymbol{A}^{I} - \boldsymbol{B}^{II}) = (\boldsymbol{A}^{I} - \boldsymbol{B}^{II})e^{-\boldsymbol{\Gamma}_p} \tag{4.18}$$

$$\boldsymbol{S}_{-}^{-1}\boldsymbol{S}_{+}\boldsymbol{\Gamma}_p(\boldsymbol{A}^{I} + \boldsymbol{B}^{II}) = \boldsymbol{\Gamma}_p(\boldsymbol{A}^{I} + \boldsymbol{B}^{II})e^{-\boldsymbol{\Gamma}_p} \tag{4.19}$$

Both equations result in the same propagation constants $\Gamma_p$ for the periodic structure.

## *4.2 Waveguide steps*

As the next problem we will analyze offsets in waveguides (see Figure 4.3).

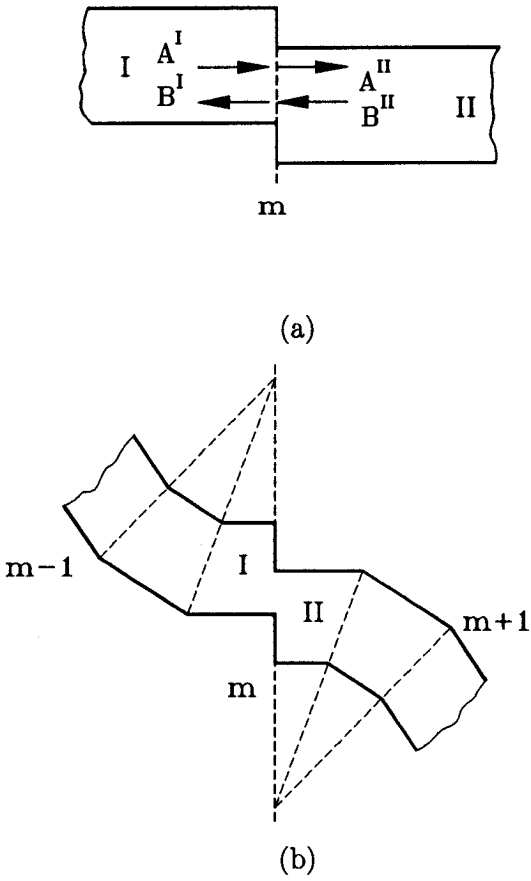


**Figure 4.3 Steps in waveguides (a) arbitrary step (b) offset in the S-bend of Figure 4.1.**

For the potential and its derivatives in plane $m$ we have

$$\phi_m^I = \hat{T}_I A^I + \hat{T}_I B^I$$

$$\phi_m^{II} = \hat{T}_{II} A^{II} + \hat{T}_{II} B^{II} \tag{4.20}$$

$$\frac{d}{d\bar{z}}\phi_m^I = -\hat{T}_I \Gamma_I A^I + \hat{T}_I \Gamma_I B^I$$

$$\frac{d}{d\bar{z}}\phi_m^{II} = -\hat{T}_{II} \Gamma_{II} A^{II} + \hat{T}_{II} \Gamma_{II} B^{II} \tag{4.21}$$

The equations are formally equal for both polarizations, and the quantities must have a subscript $e$ or $h$ for TE or TM modes, respectively.

The matching process must be done for each polarization separately. For the TM case we obtain

$$\left(\hat{\epsilon}_{rI}^{-1}\overline{h}_y^{-2}\hat{P}_{yI} - I\right)\hat{T}_I\left(A^I + B^I\right) = \left(\hat{\epsilon}_{rII}^{-1}\overline{h}_y^{-2}\hat{P}_{yII} - I\right)\hat{T}_{II}\left(A^{II} + B^{II}\right) \tag{4.22}$$

$$\hat{T}_I \Gamma_I \left(A^I - B^I\right) = \hat{T}_{II}\Gamma_{II}\left(A^{II} - B^{II}\right) \tag{4.23}$$

where $\hat{\epsilon}_r$ and $\hat{P}_y$ are according to Eqs. (2.14) and (2.23), respectively.

For the TE case we obtain

$$\left(\hat{\epsilon}_{rI}^{-1}\overline{h}_x^{-2}\hat{P}_{xI} - I\right)\hat{T}_I\left(A^I + B^I\right) = \left(\hat{\epsilon}_{rII}^{-1}\overline{h}_x^{-2}\hat{P}_{xII} - I\right)\hat{T}_{II}\left(A^{II} + B^{II}\right)$$

$$\hat{T}_I \Gamma_I \left(A^I - B^I\right) = \hat{T}_{II}\Gamma_{II}\left(A^{II} - B^{II}\right)$$

where $\hat{\epsilon}_r$ and $\hat{P}_x$ are analogous to Eqs. (2.14) and (2.23), respectively, as described in section 2.2.

With the abbreviations

$$\left(\hat{\epsilon}_{rI,II}^{-1}\overline{h}_y^{-2}\hat{P}_{yI,II} - I\right)\hat{T}_{I,II} = S_{I,II} \tag{4.26}$$

$$\hat{T}_{I,II}\Gamma_{I,II} = R_{I,II} \tag{4.27}$$

for the TM case and

$$\left(\hat{\epsilon}_{rI,II}^{-1}\bar{h}_x^{-2}\hat{P}_{xI,II} - I\right)\hat{T}_{I,II} = S_{I,II} \tag{4.28}$$

$$\hat{T}_{I,II}\Gamma_{I,II} = R_{I,II} \tag{4.29}$$

for the TE case, we obtain

$$\begin{bmatrix} S_I & S_I \\ R_I & -R_I \end{bmatrix}\begin{bmatrix} A^I \\ B^I \end{bmatrix} = \begin{bmatrix} S_{II} & S_{II} \\ R_{II} & -R_{II} \end{bmatrix}\begin{bmatrix} A^{II} \\ B^{II} \end{bmatrix} \tag{4.30}$$

This equation formally corresponds to Eq. (4.8) but note that the definitions for $S$ and $R$ are different. With $B^{II} = 0$ the solutions for the transmitted and reflected wave amplitudes are

$$A^{II} = 2\left(R_I^{-1}R_{II} + S_I^{-1}S_{II}\right)^{-1}A^I \tag{4.31}$$

$$B^I = \left(R_{II}^{-1}R_I + S_{II}^{-1}S_I\right)^{-1}\left(R_{II}^{-1}R_I - S_{II}^{-1}S_I\right)A^I \tag{4.32}$$

Especially, these formulas are valid on the offsets in the S-bend in Fig. 4.1. In this case the result e.g. from Eq. (4.13) should be used as input $A^I$.

### *4.3 Bragg Gratings*

Bragg gratings are used e.g. in filters, DFB and DBR lasers, and grating assisted couplers. Therefore in this section the formulas will be given for the analysis of the multilayered waveguide structures with an integrated Bragg grating as shown in Fig. 4.4 [33]. Because $\partial/\partial\bar{x} = 0$, we find from Eq. (2.8) for the

*TE case:*

$$\begin{aligned} \phi_e &= E_x \\ \eta_o H_y &= j\frac{\partial E_x}{\partial \bar{z}} \\ \eta_o H_z &= -j\frac{\partial E_x}{\partial \bar{y}} \end{aligned} \tag{4.33}$$

*TM case:*

$$\frac{\partial \phi_h}{\partial \bar{z}} = j\eta_o H_x$$

$$\epsilon_r E_y = -j\frac{\partial}{\partial \bar{z}}(\eta_o H_x) \tag{4.34}$$

$$\epsilon_r E_z = j\frac{\partial}{\partial \bar{y}}(\eta_o H_x)$$

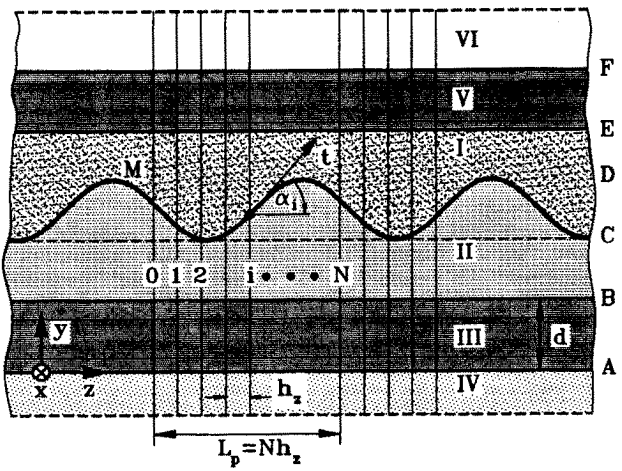


**Figure 4.4 Multilayered waveguide structure with an integrated Bragg grating.**

The wave equations are of the Helmholz type

$$\frac{\partial^2 \psi}{\partial \bar{z}^2} + \frac{\partial^2 \psi}{\partial \bar{y}^2} + \epsilon_r \psi = 0 \tag{4.35}$$

with $\psi = E_x$ or $\psi = H_x$, respectively. In the analysis of periodic structures it is convenient to normalize the field with respect to the phase in the following way [25,3]:

$$e^{jk_{\bar{z}}\bar{z}}\psi \tag{4.36}$$

$k_{\bar{z}}$ is the propagation constant in $z$ direction normalized with $k_o$. In our case the propagation constant $\gamma = \alpha + jk_z$ may be complex. In discretized form therefore we write for Eq. (4.36)

$$e^{\gamma_{\bar{z}}\bar{z}}\psi \rightarrow \boldsymbol{S}\,\boldsymbol{\psi} \tag{4.37}$$

with

$$\boldsymbol{S}_e = \mathrm{diag}(\sigma^i) \qquad \boldsymbol{S}_h = s\,\boldsymbol{S}_e \tag{4.38}$$

and

$$\sigma = e^{\gamma_{\bar{z}}\bar{h}} = s^2$$

For the phase normalized second order derivative we obtain

$$\bar{h}_z^2 e^{\gamma_{\bar{z}}\bar{z}} \frac{\partial^2 \psi}{\partial \bar{z}^2} \rightarrow -\boldsymbol{P}_p \boldsymbol{S}\, \boldsymbol{\psi} \tag{4.39}$$

where $\boldsymbol{P}_p$ is the difference operator for the periodic structure [3] and has the following form

$$\boldsymbol{P}_p = \boldsymbol{D}'_p \boldsymbol{D}_p = \begin{bmatrix} -s^{-1} & & & s \\ s & \ddots & & \\ & \ddots & \ddots & \\ & & s & -s^{-1} \end{bmatrix} \begin{bmatrix} -s & s^{-1} & & \\ & \ddots & \ddots & \\ & & \ddots & s^{-1} \\ s^{-1} & & & -s \end{bmatrix}$$

$$= \begin{bmatrix} 2 & -\sigma^{-1} & & -\sigma \\ -\sigma & \ddots & \ddots & \\ & \ddots & \ddots & -\sigma^{-1} \\ -\sigma^{-1} & & -\sigma & 2 \end{bmatrix} = \boldsymbol{D}_p \boldsymbol{D}'_p \tag{4.40}$$

$\boldsymbol{D}_p$ and $\boldsymbol{D}'_p$ are the difference operators for the derivatives of first order of $\psi_e$ and $\psi_h$, respectively. After transformation for diagonalization

$$\boldsymbol{S}\, \boldsymbol{\psi} = \boldsymbol{T}\, \overline{\boldsymbol{\psi}} \tag{4.41}$$

we obtain

$$\frac{d^2}{d\bar{y}^2} \overline{\boldsymbol{\psi}} - \boldsymbol{k}_{\bar{y}}^2 \overline{\boldsymbol{\psi}} = 0 \qquad \boldsymbol{k}_{\bar{y}}^2 = \overline{\boldsymbol{\lambda}}^2 - \epsilon_r \boldsymbol{I} \tag{4.42}$$

where

$$\boldsymbol{T}^{*t} \boldsymbol{P}_p \boldsymbol{T} = \bar{h}_z^2 \overline{\boldsymbol{\lambda}}^2 \tag{4.43}$$

and

$$x\boldsymbol{T}_{eik} = \frac{1}{\sqrt{N}} e^{ji\varphi_k}$$

$$\boldsymbol{T}_{hik} = \frac{1}{\sqrt{N}} e^{j(i+\frac{1}{2})\varphi_k}$$

$$\overline{\boldsymbol{\chi}}^2 = \bar{\boldsymbol{\delta}}\bar{\boldsymbol{\delta}}' = \bar{\boldsymbol{\delta}}'\bar{\boldsymbol{\delta}}$$

$$\bar{\boldsymbol{\delta}} = \operatorname{diag}\left(2j\overline{h}_z^{-1} \sin\frac{\varphi_k + j\gamma_{\overline{z}}\overline{h}_z}{2}\right)$$

$$\overline{\boldsymbol{\delta}'} = \operatorname{diag}\left(-2j\overline{h}_z^{-1} \sin\frac{\varphi_k + j\gamma_{\overline{z}}\overline{h}_z}{2}\right)$$

$$\varphi_k = 2\pi\frac{k}{N} \qquad k = 1, 2 \ldots N$$

The tangential fields in the planes $A$ and $B$ are related to each other as follows

$$\begin{bmatrix} \overline{\boldsymbol{F}}_{xB} \\ j\overline{\boldsymbol{F}}_{zB} \end{bmatrix} = \begin{bmatrix} \cosh \boldsymbol{k}_{\overline{y}}\overline{d} & \boldsymbol{W} \sinh \boldsymbol{k}_{\overline{y}}\overline{d} \\ \boldsymbol{W}^{-1} \sinh \boldsymbol{k}_{\overline{y}}\overline{d} & \cosh \boldsymbol{k}_{\overline{y}}\overline{d} \end{bmatrix} \begin{bmatrix} \overline{\boldsymbol{F}}_{xA} \\ j\overline{\boldsymbol{F}}_{zA} \end{bmatrix} \tag{4.44}$$

where in the

*TE case:*

$$\overline{\boldsymbol{F}}_x = \overline{\boldsymbol{E}}_x$$

$$\overline{\boldsymbol{F}}_z = \eta_0 \overline{\boldsymbol{H}}_z$$

$$\boldsymbol{W} = \boldsymbol{Z}_e = \boldsymbol{k}_{\overline{y}}^{-1}$$

*TM case:*

$$\overline{\boldsymbol{F}}_x = -\eta_0 \overline{\boldsymbol{H}}_x$$

$$\overline{\boldsymbol{F}}_z = \overline{\boldsymbol{E}}_z$$

$$\boldsymbol{W} = \boldsymbol{Z}_h^{-1} = \epsilon_r \boldsymbol{k}_{\overline{y}}^{-1}$$

With the formulas (4.44) the fields may be transformed from one plane of a homogeneous layer to the other.

Now we will consider the inhomogeneous layer between planes $C$ and $D$. For this layer the fields at the interface $M$ may be matched. With the ansatz

$$\begin{aligned}\overline{\boldsymbol{F}}_x^I &= e^{-\boldsymbol{k}_{\overline{y}}^I \overline{y}} \boldsymbol{A}^I + e^{\boldsymbol{k}_{\overline{y}}^I \overline{y}} \boldsymbol{B}^I \\ \overline{\boldsymbol{F}}_x^{II} &= e^{-\boldsymbol{k}_{\overline{y}}^{II} \overline{y}} \boldsymbol{A}^{II} + e^{\boldsymbol{k}_{\overline{y}}^{II} \overline{y}} \boldsymbol{B}^{II}\end{aligned} \tag{4.45}$$

we obtain from the matching of the component in $x$ direction:

$$\boldsymbol{S}_-^I \boldsymbol{A}^I + \boldsymbol{S}_+^I \boldsymbol{B}^I = \boldsymbol{S}_-^{II} \boldsymbol{A}^{II} + \boldsymbol{S}_+^{II} \boldsymbol{B}^{II} \tag{4.46}$$

where

$$(\boldsymbol{S}_\pm)_{ik} = (\boldsymbol{T}_{e,h})_{ik} e^{\pm(\boldsymbol{k}_{\overline{y}})_k \overline{y}_i} \tag{4.47}$$

In the tangential direction $t$ we have to match

$$\begin{aligned}\boldsymbol{H}_t &= \boldsymbol{\tau}_s \boldsymbol{H}_y + \boldsymbol{\tau}_c \boldsymbol{H}_z \\ \boldsymbol{E}_t &= \boldsymbol{\tau}_s \boldsymbol{E}_y + \boldsymbol{\tau}_c \boldsymbol{E}_z\end{aligned} \tag{4.48}$$

where

$$\boldsymbol{\tau}_s = \operatorname{diag}(\sin \alpha_i) \qquad \boldsymbol{\tau}_c = \operatorname{diag}(\cos \alpha_i)$$

The angle $\alpha_i$ for each line $i$ is defined as given in Fig. 4.4. With the Eqs. (4.3) (4.4) and (4.45) then we obtain

$$\varepsilon_{rq} \left[ \boldsymbol{R}_-^I \boldsymbol{A}^I - \boldsymbol{R}_+^I \boldsymbol{B}^I \right] = \boldsymbol{R}_-^{II} \boldsymbol{A}^{II} - \boldsymbol{R}_+^{II} \boldsymbol{B}^{II} \tag{4.49}$$

where

$$\boldsymbol{R}_\pm^{I,II} = \boldsymbol{\tau}_c \boldsymbol{S}_\pm^{I,II} \boldsymbol{k}_{\overline{y}}^{I,II} \mp \boldsymbol{\tau}_s \boldsymbol{S}_\pm^{I,II} \overline{\boldsymbol{\delta}} \tag{4.50}$$

with $\epsilon_{rq} = 1$ for the TE case and $\epsilon_{rq} = \epsilon_r^I / \epsilon_r^{II}$ for the TM case.

With the formulas (4.45), (4.46), and (4.49) the transformation of the field components between planes $B$ and $E$ or $C$ and $D$ is described. To obtain well conditioned matrices $\boldsymbol{S}_\pm$, the origin of the $y$ axis should be chosen in the middle between $C$ and $D$.

With the equations given above an indirect eigenvalue problem can be now formulated in the form

$$\boldsymbol{R}\,\overline{\boldsymbol{F}}_x = \boldsymbol{0}$$

for an arbitrarily plane, e.g. plane B. From the condition $\det(\boldsymbol{R}) = 0$ the propagation constant $\gamma_{\bar{z}}$ will be found and then the eigenvector $\overline{\boldsymbol{F}}_x$ can be calculated.

## 5. Algorithm for Vectorial Field

In this case the two coupled Sturm-Liouville equations (2.5) and (2.6) must be solved

$$L^{(e)}\boldsymbol{\phi}_e = \epsilon_r^{-1}\frac{\partial \epsilon_r}{\partial \bar{x}}\frac{\partial \boldsymbol{\phi}_h}{\partial \bar{y}} \tag{5.1}$$

$$L^{(h)}\boldsymbol{\phi}_h = \epsilon_r^{-1}\frac{\partial \epsilon_r}{\partial \bar{y}}\frac{\partial \boldsymbol{\phi}_e}{\partial \bar{x}} \tag{5.2}$$

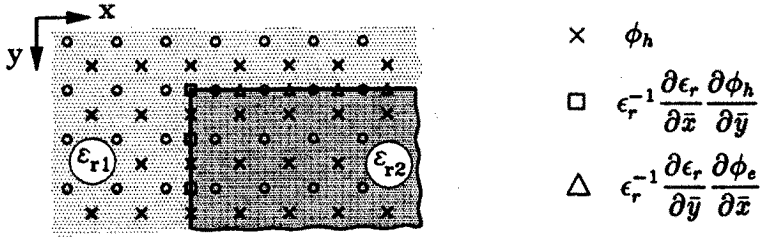


**Figure 5.1 The positions of discretization points for the potentials and for the coupling terms.**

In Figure 5.1 the positions of discretization points not only for the potentials but also for the coupling terms are sketched. As can be seen, the coupling terms are only nonzero at the interfaces. The coupling term in the first equation results from vertical interfaces (or horizontal

changes of $\epsilon_r$) and the coupling term in the second equation results from horizontal interfaces (or vertical changes of $\epsilon_r$). The places of discretization of the coupling terms are different from those of the potentials. Therefore the coupling terms should be rewritten in the following form [26]

$$\epsilon_r^{-1}\frac{\partial\epsilon_r}{\partial\bar{x}}\frac{\partial\phi_h}{\partial\bar{y}} = \frac{\partial^2\phi_h}{\partial\bar{x}\partial\bar{y}} - \epsilon_r\frac{\partial}{\partial\bar{x}}\left(\epsilon_r^{-1}\frac{\partial\phi_h}{\partial\bar{y}}\right) \tag{5.3}$$

$$\epsilon_r^{-1}\frac{\partial\epsilon_r}{\partial\bar{y}}\frac{\partial\phi_e}{\partial\bar{x}} = \frac{\partial^2\phi_e}{\partial\bar{y}\partial\bar{x}} - \epsilon_r\frac{\partial}{\partial\bar{y}}\left(\epsilon_r^{-1}\frac{\partial\phi_e}{\partial\bar{x}}\right) \tag{5.4}$$

Because we have mixed second order derivatives on the right side now, we obtain the discretized coupling terms on the points for the potentials. The discretized wave equations now run as follows:

$$\frac{d^2}{d\bar{z}^2}\begin{bmatrix}\hat{\phi}_e\\ \hat{\phi}_h\end{bmatrix} - \begin{bmatrix}\hat{Q}_e & \hat{U}_h\\ \hat{U}_e & \hat{Q}_h\end{bmatrix}\begin{bmatrix}\hat{\phi}_e\\ \hat{\phi}_h\end{bmatrix} = \mathbf{0} \tag{5.5}$$

with

$$\hat{Q}_e = \bar{h}_y^{-2}\hat{P}_{ye} + \bar{h}_x^{-2}\hat{P}_{xe} - \hat{\epsilon}_{re} \tag{5.6}$$

$$\hat{Q}_h = \bar{h}_y^{-2}\hat{P}_{yh} + \bar{h}_x^{-2}\hat{P}_{xh} - \hat{\epsilon}_{rh} \tag{5.7}$$

where $\hat{P}_x$, $\hat{P}_y$ and $\hat{\epsilon}_r$ are constructed as described in section 2.2 and $\hat{U}_e$ and $\hat{U}_h$ are the discretized coupling terms

$$\hat{U}_h = (\bar{h}_x\bar{h}_y)^{-1}\cdot(\hat{D}_x^t\hat{D}_y^a - \hat{\epsilon}_{re}\hat{D}_x^t\hat{\epsilon}_{rhe}^{-1}\hat{D}_y^a) \tag{5.8}$$

$$\hat{U}_e = (\bar{h}_x\bar{h}_y)^{-1}\cdot(\hat{D}_y^t\hat{D}_x^a - \hat{\epsilon}_{rh}\hat{D}_y^t\hat{\epsilon}_{reh}^{-1}\hat{D}_x^a) \tag{5.9}$$

with

$$\hat{D}_y^a = I_x^h \otimes D_y^a \qquad \hat{D}_y^t = I_x^h \otimes D_y^t$$

$$\hat{D}_x^a = D_x^a \otimes I_y^e \qquad \hat{D}_x^t = D_x^t \otimes I_y^e$$

$D_x$ and $D_y$ are constructed as described in section 2.2. $\hat{\epsilon}_{reh}$ is constructed analogously to $\hat{\epsilon}_{rhe}$. The results are equal. The transformation for the diagonalization of the block matrix in Eq.( 5.5) is done

in the following way:

$$\hat{\boldsymbol{\phi}} = \begin{bmatrix} \hat{\boldsymbol{\phi}}_e \\ \hat{\boldsymbol{\phi}}_h \end{bmatrix} = \begin{bmatrix} \hat{\boldsymbol{T}}^e & \hat{\boldsymbol{T}}^{eh} \\ \hat{\boldsymbol{T}}^{he} & \hat{\boldsymbol{T}}^h \end{bmatrix} \begin{bmatrix} \hat{\tilde{\boldsymbol{\phi}}}_e \\ \hat{\tilde{\boldsymbol{\phi}}}_h \end{bmatrix} = \hat{\tilde{\boldsymbol{T}}}\,\hat{\tilde{\boldsymbol{\phi}}} \tag{5.10}$$

where

$$\hat{\tilde{\boldsymbol{T}}}^{-1} \begin{bmatrix} \hat{\boldsymbol{Q}}_e & \hat{\boldsymbol{U}}_h \\ \hat{\boldsymbol{U}}_e & \hat{\boldsymbol{Q}}_h \end{bmatrix} \hat{\tilde{\boldsymbol{T}}} = \hat{\tilde{\boldsymbol{\Gamma}}}^2 \tag{5.11}$$

With the matrix of propagation constants $\hat{\tilde{\boldsymbol{\Gamma}}}$ the propagation is described by

$$\hat{\tilde{\boldsymbol{\phi}}}(z) = \begin{bmatrix} \hat{\tilde{\boldsymbol{\phi}}}_e(z) \\ \hat{\tilde{\boldsymbol{\phi}}}_h(z) \end{bmatrix} = e^{-\boldsymbol{P}\overline{z}} \begin{bmatrix} \hat{\tilde{\boldsymbol{\phi}}}_e(0) \\ \hat{\tilde{\boldsymbol{\phi}}}_h(0) \end{bmatrix} = e^{-\boldsymbol{P}\overline{z}}\,\hat{\tilde{\boldsymbol{\phi}}}(0) \tag{5.12}$$

in one direction and by

$$\hat{\tilde{\boldsymbol{\phi}}} = e^{-\boldsymbol{P}\overline{z}}\boldsymbol{A} + e^{\boldsymbol{P}\overline{z}}\boldsymbol{B} \tag{5.13}$$

in both directions.

With the abbreviations

$$\hat{\boldsymbol{H}} = \eta_o \begin{bmatrix} -j\hat{\boldsymbol{H}}_y \\ j\hat{\boldsymbol{H}}_x \end{bmatrix} \qquad \hat{\boldsymbol{E}} = \begin{bmatrix} \hat{\boldsymbol{E}}_x \\ \hat{\boldsymbol{E}}_y \end{bmatrix} \tag{5.14}$$

the solution for the field is given by

$$\hat{\boldsymbol{H}} = \frac{\partial}{\partial \overline{z}} \hat{\boldsymbol{\phi}}$$

$$\hat{\boldsymbol{H}} = -\boldsymbol{R}\left(e^{-\hat{\tilde{\boldsymbol{\Gamma}}}\overline{z}}\boldsymbol{A} - e^{\hat{\tilde{\boldsymbol{\Gamma}}}\overline{z}}\boldsymbol{B}\right) \tag{5.15}$$

$$\hat{\boldsymbol{E}} = -\boldsymbol{S}\left(e^{-\hat{\tilde{\boldsymbol{\Gamma}}}\overline{z}}\boldsymbol{A} + e^{\hat{\tilde{\boldsymbol{\Gamma}}}\overline{z}}\boldsymbol{B}\right) \tag{5.16}$$

and

$$\boldsymbol{R} = \hat{\hat{\boldsymbol{T}}}\hat{\hat{\boldsymbol{\Gamma}}}$$

$$\boldsymbol{S} = \begin{bmatrix} \hat{\boldsymbol{\epsilon}}_{re}^{-1}\overline{h}_x^{-2}\hat{\boldsymbol{P}}_{xe} - \boldsymbol{I}_e & \hat{\boldsymbol{D}}_x^t\hat{\boldsymbol{\epsilon}}_{rhe}^{-1}\hat{\boldsymbol{D}}_y^a \\ \hat{\boldsymbol{D}}_y^t\hat{\boldsymbol{\epsilon}}_{reh}^{-1}\hat{\boldsymbol{D}}_x^a & \hat{\boldsymbol{\epsilon}}_{rh}^{-1}\overline{h}_y^{-2}\boldsymbol{P}_{yh} - \boldsymbol{I}_h \end{bmatrix} \hat{\hat{\boldsymbol{T}}} \tag{5.17}$$

By using these extended definitions for $\boldsymbol{R}$ and $\boldsymbol{S}$ instead of those in (4.26) to (4.29), the results in Eqs. (4.31) and (4.32) are valid for vectorial fields, too.

With the Eqs. (5.15) and (5.16) also the algorithm in 4.1 may be extended for vectorial fields. Formally the same results as in Eq. (4.8) will be obtained. But now the quantities must be defined according to

$$(\boldsymbol{S}_\pm)_{n,n'} = (\boldsymbol{S})_{n,n'}\, e^{\mp(\hat{\hat{\boldsymbol{\Gamma}}})_{n'}\Delta\overline{z}_n} \tag{5.18}$$

$$(\boldsymbol{R}_\pm)_{n,n'} = (\boldsymbol{R})_{n,n'}\, e^{\mp(\hat{\hat{\boldsymbol{\Gamma}}})_{n'}\Delta\overline{z}_n} \tag{5.19}$$

Instead of $\tau_e$ and $\tau_h$ the quantities $\hat{\boldsymbol{\tau}}_e$ and $\hat{\boldsymbol{\tau}}_h$ must be used where

$$\begin{aligned} \hat{\boldsymbol{\tau}}_e &= \mathrm{Diag}(\tau_e\boldsymbol{I}_e,\ \boldsymbol{I}_h) \\ \hat{\boldsymbol{\tau}}_h &= \mathrm{Diag}(\boldsymbol{I}_e,\ \tau_h\boldsymbol{I}_h) \end{aligned} \tag{5.20}$$

$\Delta\overline{z}_n$ varies two times as in (4.9) according to the discretization lines of the two potentials.

## 6. Results

In this chapter some typical results shall be presented. For the others, e.g. for the $Y$ junction or a waveguide diode transition, the reader may be referred to the literature [18–21, 31,32]. First it is shown how well the absorbing boundary conditions work. In Fig. 6.1 the propagation of a Gaussian beam in a homogeneous medium towards the boundary under an angle of 45 degrees with implemented ABCs is demonstrated. The figure shows the beam in different positions beginning with the starting position. No reflections can be seen if the beam propagates through the boundary.

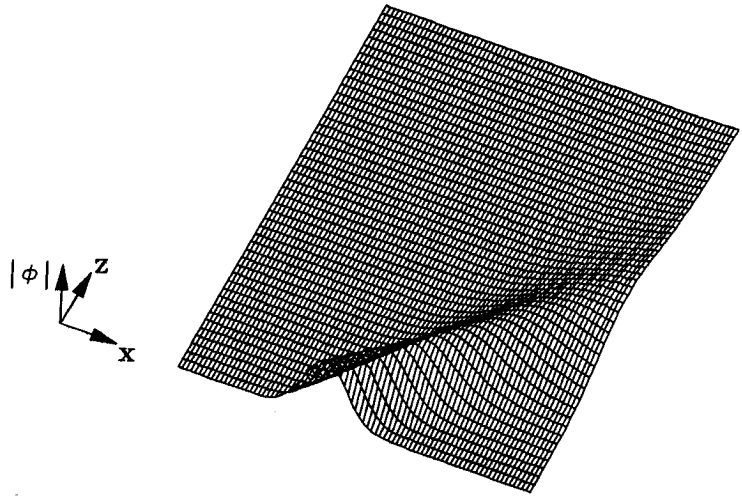


**Figure 6.1 Propagation of a Gaussian beam in free space towards the absorbing boundary under an angle of incidence of $\theta = 45°$.**

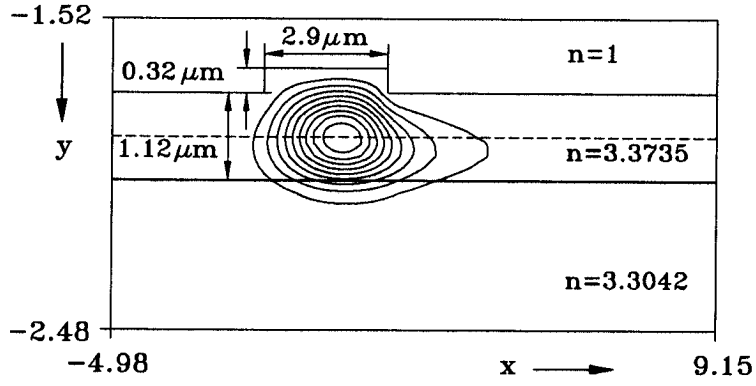


**Figure 6.2 Intensity distribution of the lowest order quasi–TE mode in a waveguide bend (Bend radius $R_o = 2\text{mm}, \lambda = 1.52\mu\text{m}$. ©IEE 1994.**

Next some results for a rib waveguide bend will be presented [36]. Figure 6.2 shows the intensity distribution in the cross section for the lowest order quasi–TE mode. The bend is curved to the left and the diagram clearly shows the shift to the right. The result may be compared with that obtained by Gu [27]. For another waveguide a vectorial solution was obtained by Pascher and Pregla [28]. In both cases the distribution is equal in the main part. Only on the right outer side there are some small differences.

To show that the MoL yields accurate field behavior we have calculated the $E_x$ component of this mode in the half rib height as a function of $x$. The normalized component is drawn in Fig. 6.3. Also in this curve the shift of the field to the right can be seen. As can be seen, also the jump in the permittivity is modeled properly. This is because self-adjoint formulation of the wave equation is used and interface conditions are introduced appropriately. This curve is also nearly insensitive to the number of discretization points. This behavior is according to the fact that the MoL is related to the discrete Fourier transformation which gives correct values on the discretization points for a periodic function.

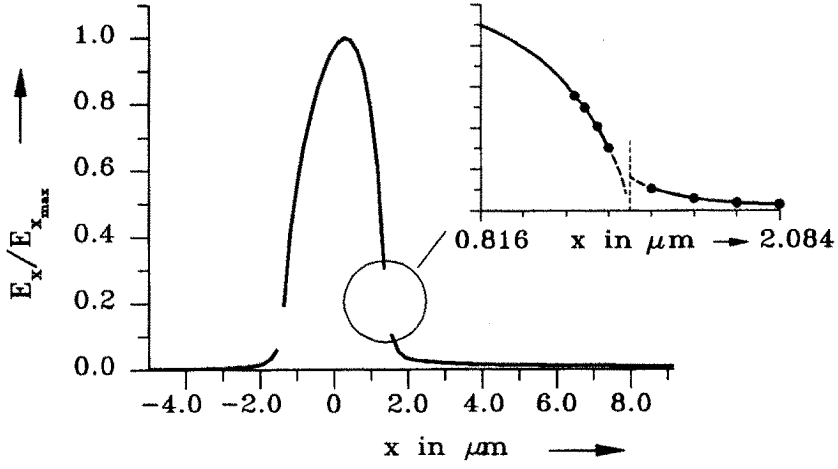


**Figure 6.3 Normalized $E_x$ component of the lowest order quasi TE mode.**

The diagram in Fig. 6.4 shows the propagation in the dashed plane (see Figure 6.2) as a function of the angle. The diagram was straightened. The propagation starts with a Gaussian distribution. After a transient process in a sector of about 7 degrees a stationary behavior is obtained. The diagram in Fig. 6.5 finally shows the loss versus the propagation angle $\Theta$. As input again a Gaussian field distribution is used. After some degrees of propagation a straight curve is obtained. The radiation loss per degree is constant. The loss calculated by Gu [27] is about 13.5 dB, the loss measured by Deri et al. [29] is about 10.5 dB, the result obtained with MoL-BPM is 11.8 dB.

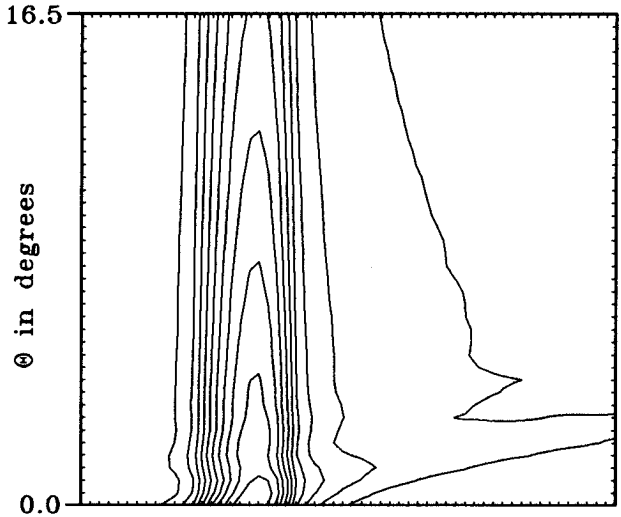


**Figure 6.4 Field distribution in the dashed plane (Figure 6.2) with a Gaussian beam as input.** 

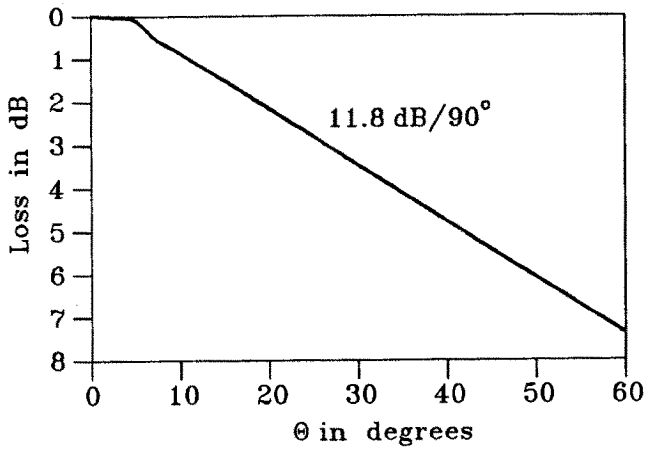


**Figure 6.5 Loss of the quasi – TE mode in a bend with a Gaussian beam as input. ($R_0 = 2\text{mm}, \lambda = 1.52\mu\text{m}$) © IEE 1993.**

The algorithm presented was also used for a circular bend of a more complicated waveguide. The cross section of that waveguide has no straight border lines (see Figures 6.6a: such waveguides are fabricated at the Technical University Hamburg-Harburg in the institute of Prof. J. Müller). At the free space wavelength $\lambda_o = 0.81\mu$ m the waveguide is multimoded. In Fig. 6.6b the intensity distribution for the 5th higher order mode with TE polarization is given. Because of the higher order modes the loss curve against the propagation angle has a ripple. The periodicity of the ripple coincides with the beat length of the fundamental mode and the first higher order mode. The dependence of the loss from curvature radius is given in the following table:

| bend radius mm | Loss dB/90° |
|---|---|
| 1.0 | 0.0277 |
| 0.5 | 0.0227 |
| 0.25 | 0.0369 |
| 0.125 | 0.127 |

Dependence of the loss from the curvature radius of the waveguide in Fig. 6.6a.

(a)

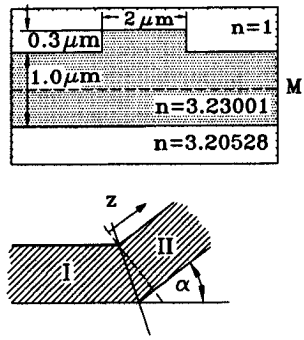


(b)

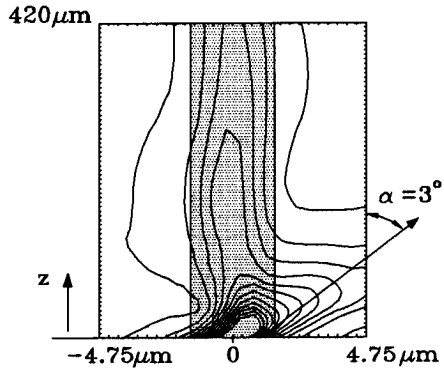


(c)

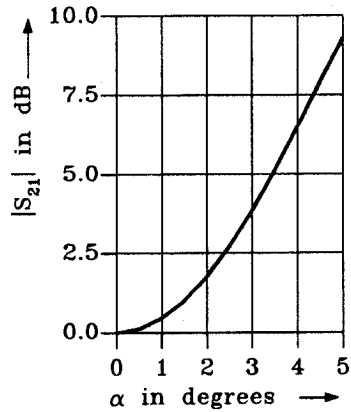


**Figure 6.6 Waveguide with non straight border lines a) Cross section of the waveguide b) Intensity distribution of the 5th order higher mode (TE polarization) c) Loss versus propagation angle.**

Figure 6.7 shows the result for a sharp waveguide bend with the bend angle $\alpha$. Dimensions and material parameters are given in figure (a). The calculations are three-dimensional. The diagram (b) shows the intensity distribution in the plane $M$ for the outgoing waveguide II. In the incoming waveguide I the fundamental TE eigenmode is propagated. It is seen that a part of the field is initially radiated in the direction of the incoming waveguide. The diagram (c) gives the transmission loss as function of the bend angle $\alpha$. All this loss is due to the radiated power, because the reflections are very small and negligible.

The Figure 6.8 shows the propagation constant $\gamma = \alpha + j\beta$ in a Bragg grating as a function of the free space wave number $k_0$. All quantities are normalized with the length $\Lambda$ of the period of the gratings. The results are obtained with two alternative procedures. In one case discretization is done in $z$ direction and in the other in $y$ direction. Excellent agreement was found between the two results.

In Figure 6.9 the result for a Bragg grating with sinusoidal contour is given in comparison to the rectangular shaped one. The dimensions and parameters are the same as in Fig. 6.8. Only the $\alpha$ curve in the stop band is drawn. As can be seen, the $\alpha$ values are reduced. This is because the reflections in the sinusoidal contour are smaller.

Figure 6.10 shows the intensity distributions in a waveguide for different offsets. The cross section and the material parameters are the same as in Fig. 6.7a. The field is plotted for the outgoing waveguide. The wave in the incoming waveguide is the fundamental TE mode. As can be seen the patterns do not change much. Therefore the loss for the total field is small (see Figure 6.11), whereas the loss for the fundamental mode is high because only a part of the total field is coupled to the outgoing waveguide .

To verify the vectorial algorithm, a polarization converter [34](see Figure 6.12) was analyzed [35]. As input wave the fundamental TE mode was used. Figure 6.13 shows the distribution at $z = 0$. As can be seen in Fig. 13b, this quasi TE mode has $E_y$ components, too. This component is obtained at the edges of the channel guide. This is necessary because the field must have poles at these points as it is well known.

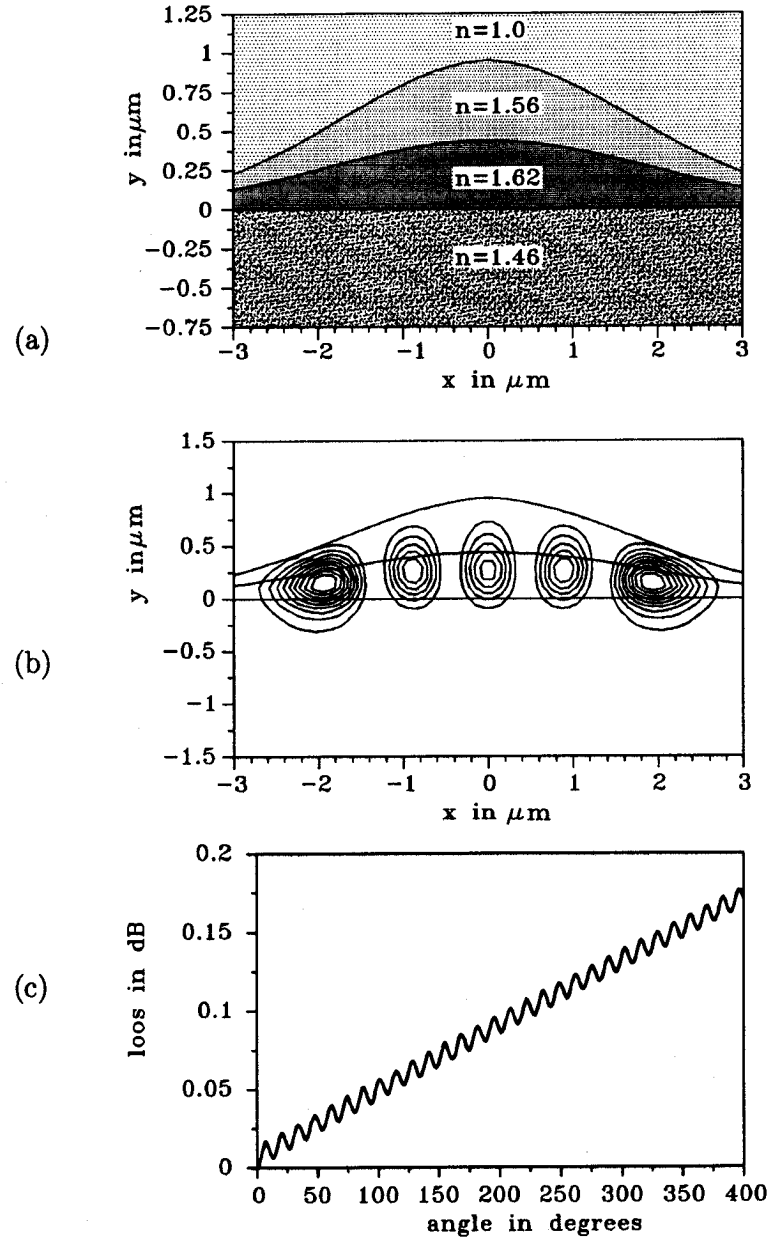


**Figure 6.7 Intensity distribution for the outgoing waveguide in the plane $M$ of a sharp waveguide bend (bend angle $\alpha$) and transmission loss as function of bend angle $\alpha$. © IEE 1993.**

(a)

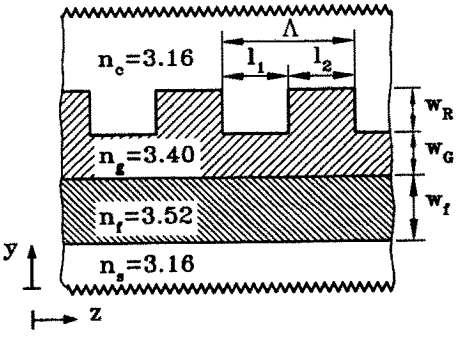


$w_R$=0.1 $\mu$m $\lambda$ =1.55 $\mu$m

$w_G$=0.1 $\mu$m $l_1$=$l_2$

$w_f$=0.15 $\mu$m

(b)

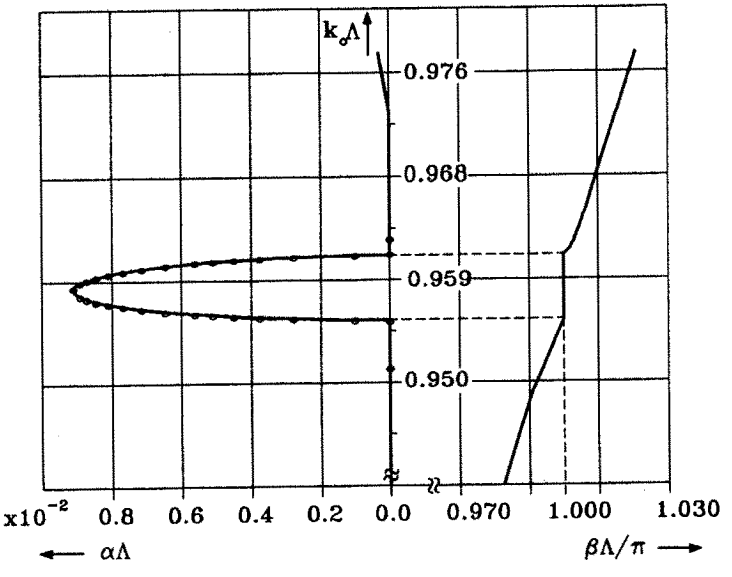


**Figure 6.8 (a) Contour of a Bragg grating with dimensions (b) Dispersion diagram © IEE 1993. ——discretization lines in $z$ direction, * * * discretization lines in $y$direction.**

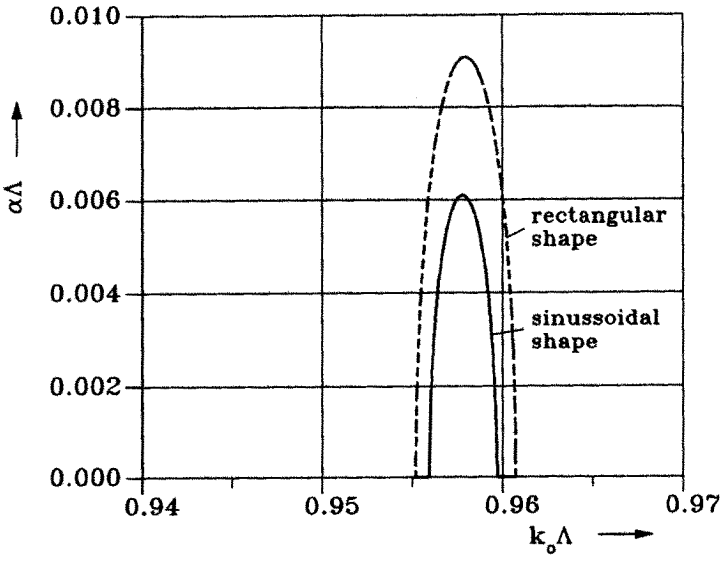


**Figure 6.9 Behavior of a sinusoidal Bragg grating in comparison with a rectangular one. © IEE 1993.**

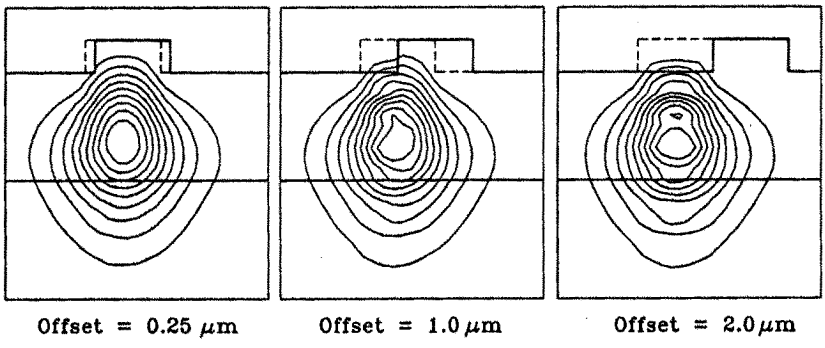


**Figure 6.10 Intensity distribution in the outgoing waveguide of a waveguide offset.**

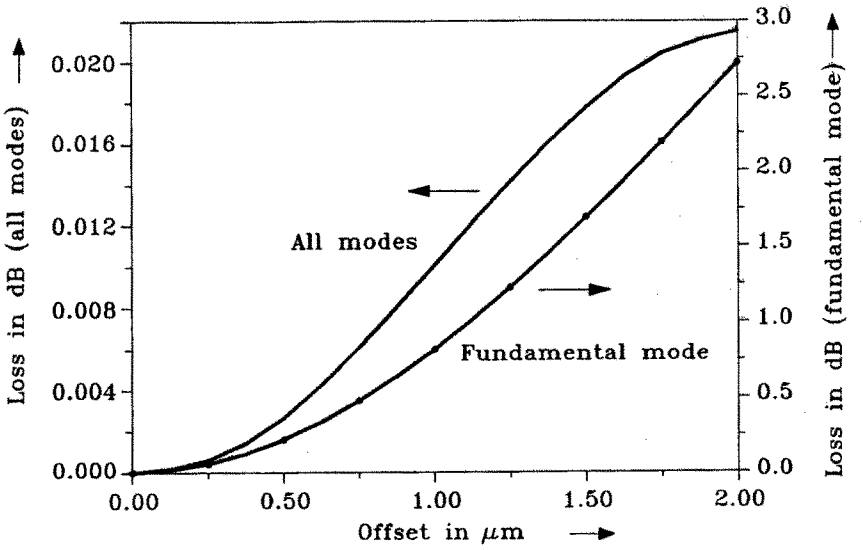


**Figure 6.11 Loss at a waveguide offset as a function of the offset width. © IEE 1993.**

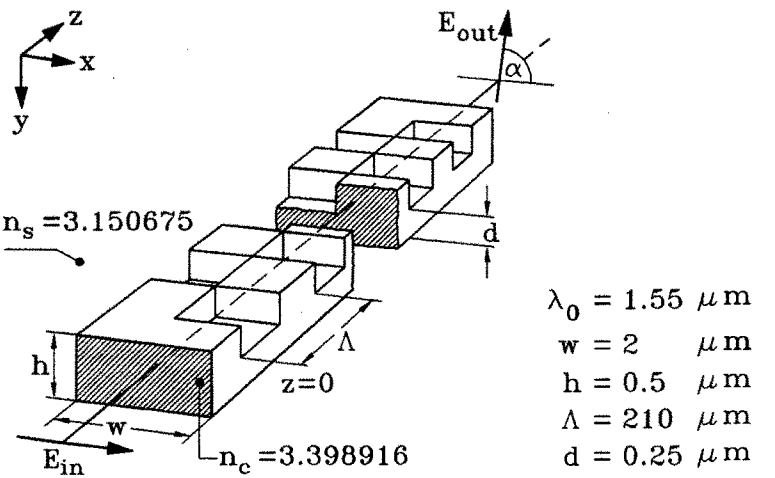


**Figure 6.12 Structure of the analyzed polarization converter [34]. © IEE 1994.**

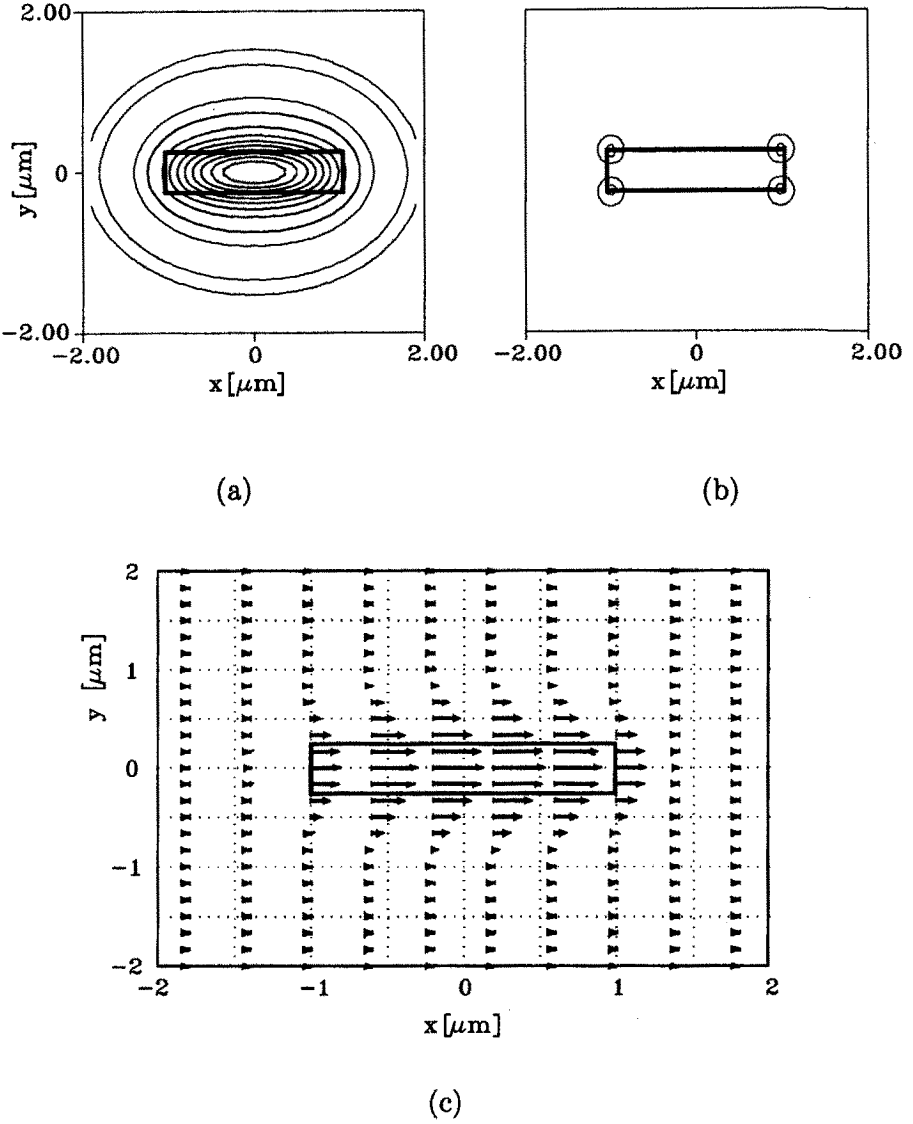


**Figure 6.13 Input field of the polarization converter a) absolute value of the $E_x$ component b) absolute value of the $E_y$ component c) vector plot.**

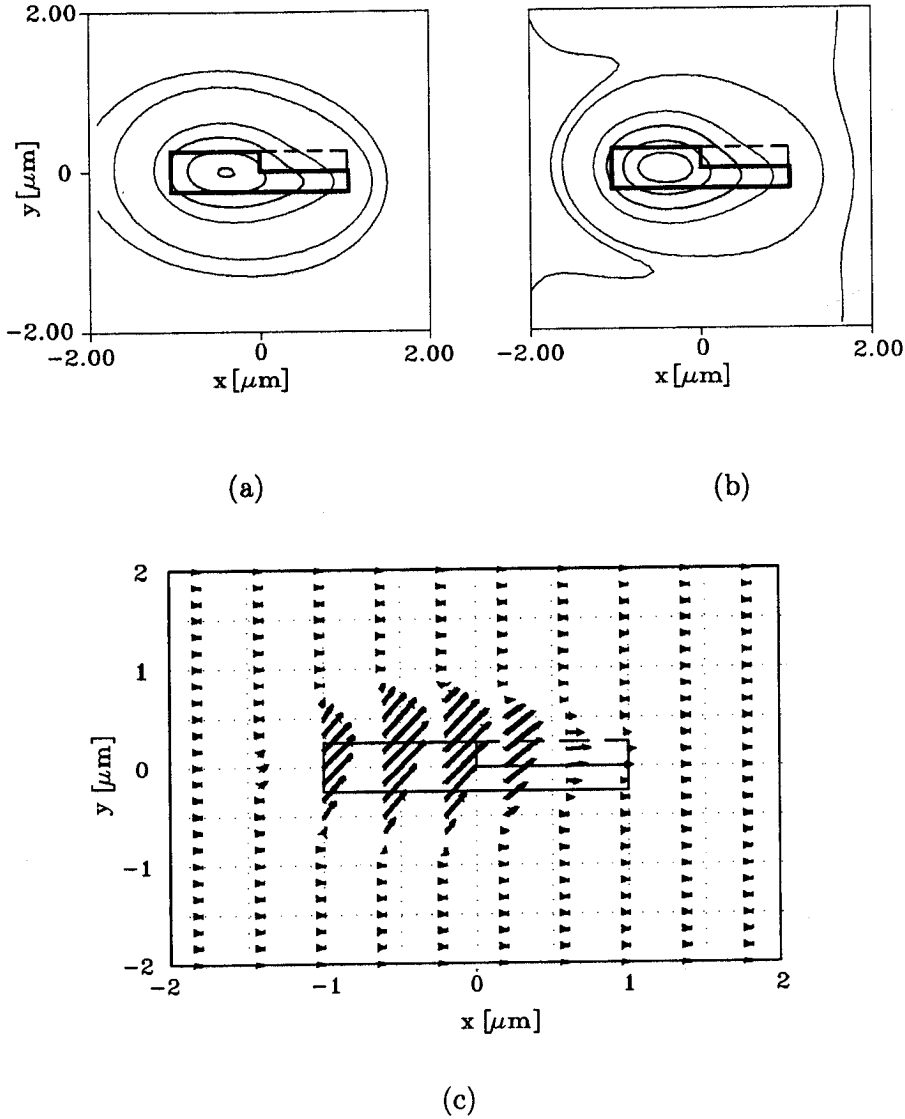


**Figure 6.14 Field distribution of the polarization converter at $z = 5\Lambda$ a) absolute value of the $E_x$ component b) absolute value of the $E_y$ component c) vector plot. © IEE 1993.**

The wave propagates in $z$ direction and the field vector rotates more and more in $y$ direction. At the position $z = 5\Lambda$ the situation is visualized in Fig. 6.14. Nearly the whole field has a distribution of about 50 degrees towards the $x$ axis.

The Figures 13 and 14 show that physically correct, smooth field plots are obtained with the described algorithm. The reason for this fact is that the formulation of wave equations is self-adjoint and interface conditions for all components are fulfilled at all interfaces. Because of this fact the method of lines is able to model the field near the singularities. This was demonstrated with numerical results by A. Kornatz in Fig. 6.15.

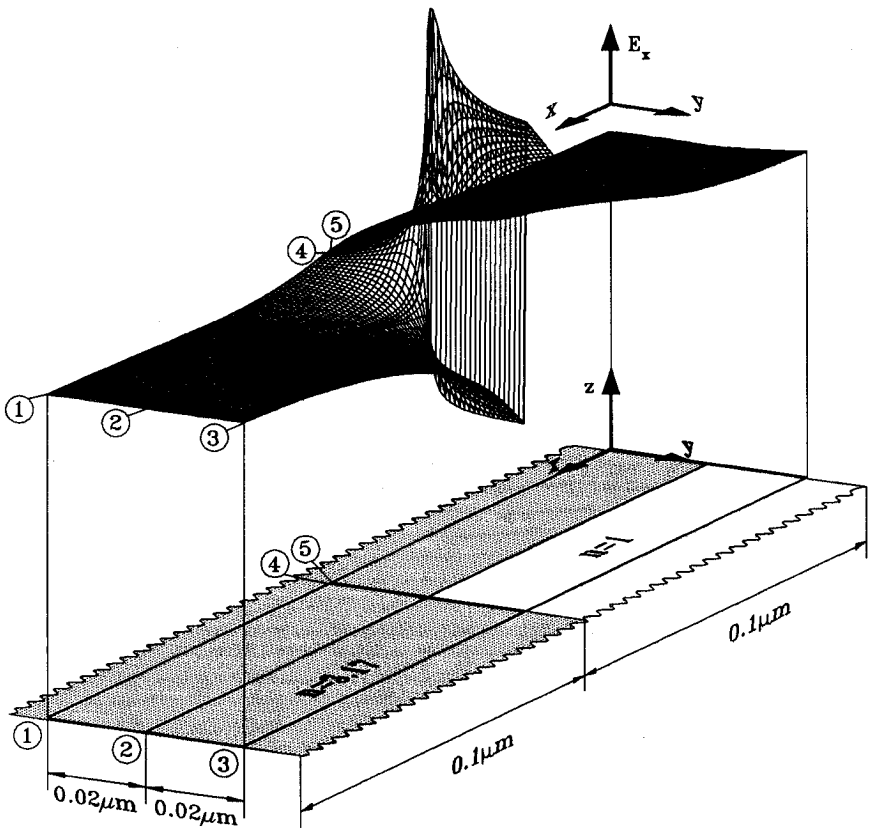


**Figure 15. Field component $E_x$ of the lowest order quasi TE mode at the dielectric edge of a rib waveguide.**

## Acknowledgment

All the numerical work for the results was done by the coworkers of the author. Therefore the author gracefully acknowledges this great help and other support of E. Ahlers, J. Gerdes, S. Helfert, A. Kornatz, D. Kremer, W. Pascher, and W. Yang.

## References

1. Liskovets, O. A., "The method of lines (English Translation)," *J. Diff. Eqs.*, Vol. 1, 1308, 1965.
2. Schulz, U., and R. Pregla, "A new technique for the analysis of the dispersion characteristics of planar waveguides," *Archiv Electronik Übertragungstechnik, (Electronics and Communication)*, AEÜ 34, 169–173, 1980.
3. Pregla, R., and W. Pascher, *"The Method of Lines,"* in T. Itoh, (editor), Numerical Techniques for Microwave and Millimeter Wave Passive Structures, 381–446, J. Wiley Publ., New York, 1989.
4. Pregla, R., and F.-J. Schmückle, "The method of lines for the analysis of lossy millimeter wave structures (in German)," *Kleinheubacher Berichte*, Vol. 32, 261–269, 1989.
5. Schmückle, F.-J., and R. Pregla, "The method of lines for the analysis of lossy planar waveguides," *IEEE Trans. Microwave Theory Tech.*, Vol. MTT-38, 1473–1479, 1990.
6. Pregla, R., M. Koch, and W. Pascher, "Analysis of hybrid waveguide structures consisting of microstrip and dielectric waveguides," *Proc. 17th Eur. Microwave Conf.*, Rome, 927–932, 1987.
7. Rogge, U., and R. Pregla, "Method of lines for the analysis of strip-loaded optical waveguides," *J. Optical Society of America B*, Vol. 8, No. 2, 459–463, 1991.
8. Rogge, U., and R. Pregla, "Method of lines for the analysis of dielectric waveguides," *J. Lightwave Technology*, Vol. 11, No. 12, 1993.
9. Feit. M. D., and J. A. Fleck, "Light propagation in graded-index optical fibers," *Appl. Opt.*, Vol. 17, 3990–3998, 1978.
10. Moore, T. G., J. G. Blaschak, A. Taflove, and G. A. Kriegsmann, "Theory and application of radiation boundary operators," *IEEE Trans. Antennas Propagation*, Vol. 36, No. 12, 1797–1811, 1988.

11. Pregla, R., and J. Gerdes, "New beam-propagation algorithm based on the method of lines," *Integrated Photonics Research, Technical Digest Series*, Vol. 5, 29–30, 1990.
12. Dreher, A., and R. Pregla, "Analysis of planar waveguides with the method of lines and absorbing boundary conditions," *IEEE Microwave Guided Wave Lett.*, Vol. 1, No. 6, 138–140, 1991.
13. Pregla, R., and D. Kremer, "Method of lines with special absorbing boundary conditions — analysis of weakly guiding optical structures," *IEEE Microwave Guided Wave Lett.*, Vol. 2, No. 6, 239–241, 1992.
14. Dreher, A., and R. Pregla "Full-wave analysis of radiating planar resonators with the method of lines," *IEEE Transactions on Microwave Theory and Technology*, Vol. 41, No. 8, 1993.
15. Dreher, A., *The method of lines and the integral equation technique for the analysis of planar antennas (in German)*, Ph.D. Dissertation, Fern Universität, Hagen, VDI-Verlag, Vol. 21, No. 116, 1991.
16. Hadley, G. R., "Transparent boundary condition for beam propagation," *Opt. Lett.*, Vol. 16, No. 9, 624–626, 1991.
17. Hadley, G. R., "Transparent boundary condition for the beam propagation method," *IEEE J. Quantum Electronics*, Vol. 28, No. 1, 363–370, 1992.
18. Gerdes, J., and R. Pregla, "Beam-propagation algorithm based on the method of lines," *J. Optical Society of America B*, Vol. 8, No. 2, 389–394, 1991.
19. Gerdes, J., R. Pregla, "New applications and improvements of the method of lines beam-propagation method," in *Integrated Photonics Research, Technical Digest Series*, Vol. 8, 93, 1991.
20. Gerdes, J., B. Lunitz, D. Benish, and R. Pregla, "Analysis of slab waveguide discontinuities including radiation and absorption effects," *Electronic Letters*, Vol. 28, 1013 – 1014, 1992.
21. Pregla, R., J. Gerdes, E. Ahlers, and S. Helfert, "MoL-BPM algorithms for waveguide bends and vectorial fields," *Integrated Photonic Research, Technical Digest Series*, Vol. 10, 32–33, 1992.
22. Collin, R. E., *Field Theory of Guided Waves*, Mc Graw-Hill, New York, 232–244, 1960.
23. Kornatz, A., and R. Pregla, "Increase of the order of approximation and improvement of the interface conditions for the method of lines," *IEEE J. Lightwave Technology*, Vol. 11, No. 2, 1993.

24. Lagasse, P., et al., "COST-216 Comparative Study of S-bend and Directional Coupler Analysis Methods," *Proc. 16th Eur. Conf. Optical Communication* Nijhoff, Amsterdam, Vol. 1, 175–178, 1990.
25. Worm, S. B., *Analysis of arbitrarily shaped planar microwave stuctures*, (in German), Ph. D. Dissertation, FernUniversität Hagen, 1983
26. Gerdes, J., *An efficient analysis of longitudinally varying integrated optical waveguides* (in German), Ph. D. Dissertation, FernUniversität, Hagen, VDI-Verlag, ISBN 3-18-143821-9, Vol. 21, No. 138, 1993
27. Gu, Jing-Son, *Numerical analysis of directionally varying optical waveguides*, Ph. D. Dissertation, ETH Zürich, chapter 6.2, 1991.
28. Pascher, W., and R. Pregla, "Analysis of curved optical waveguides by the vectorial method of lines," *Proc. Intl. Conf. Integrated Optics and Optical Fibre Communications*, 237–240, Paris, 1991.
29. Deri, R. J., and R. J. Hawkins, "Polarization, scattering and coherent effects in semiconductor Rib waveguide bends," *Opt. Letters*, Vol. 13, No. 10, 922–924, 1988.
30. Pregla, R., and E. Ahlers, "Method of lines for analysis of discontinuities in optical waveguides," *Electronics Letters*, Vol. 29, No. 21, 1845–1846, 1993.
31. Ahlers, E., and R. Pregla, "Modelling of Y–branches with the MoL–BPM", *Proceedings of the Integrated Photonics Research Topical Meeting*, San Franzisco, USA, 222–224, 1994.
32. Ahlers, E., and R. Pregla, "Modeling of Y–branches with the MoL–BPM", *Proceedings of the International Symposium on Integrated Optics*, EUROPTO series (EOS and SPIE), Lindau, Germany, 1994.
33. Pregla, R., and W. Yang, "Method of lines for analysis of multilayered dielectric waveguides with Bragg gratings," *Electronics Letters*, Vol. 29, No. 22, 1962–1963, 1993.
34. Mustieles, F. J., E. Ballesteros, and F. Hernández-Gil, "Multimodal analysis method for the design of passive TE/TM converters in integrated waveguides," *IEEE Photonics Letters,* Vol. 5, No. 7, 1993.

35. Gerdes, J., S. Helfert, and R. Pregla, "Three-dimensional vectorial eigenmode algorithm for nonparaxial propagation in reflecting optical waveguide structures," *Electronics Letters,* Vol. 31, No. 1, 65–66, 1995.
36. Pregla, R., and E. Ahlers, "Method of lines for analysis of arbitrarily curved waveguide bends," *Electronics Letters,* Vol. 30, No. 18, 1478–1479, 1994.